ESD-MSFC-2145

Interim Report

RESEARCH IN SOLAR PHYSICS: ANALYSIS OF SKYLAB/ATM S-056 X-RAY DATA

October 1977

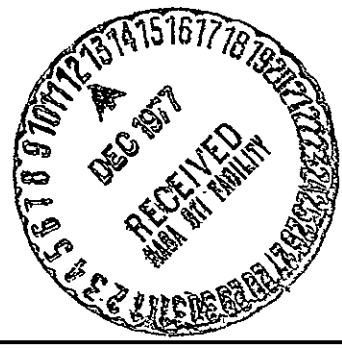

TELEDYNE BROWN ENGINEERING

Cummings Research Park • Huntsville, Alabama 35807

INTERIM REPORT
ESD-MSFC-2145

RESEARCH IN SOLAR PHYSICS: ANALYSIS OF SKYLAB/ATM S-056 X-RAY DATA

By

W. Henze, Jr., Ph.D.

October 1977

Prepared For

SPACE SCIENCES LABORATORY
GEORGE C. MARSHALL SPACE FLIGHT CENTER
HUNTSVILLE, ALABAMA

Contract No. NAS8-31908

Prepared By

ENGINEERING SERVICES DIVISION
TELEDYNE BROWN ENGINEERING
HUNTSVILLE, ALABAMA

ABSTRACT

Results of research in solar physics are presented relating to observations obtained by the S-056 X-Ray Experiment on Skylab. Included are a description of the X-Ray Event Analyzer (X-REA) data, a summary of the film calibration, analyses of the 15 June 1973 flare, results of a study of oscillations in the solar soft X-ray flux, and results of an investigation into deconvolution of X-ray images of the 5 September 1973 flare.

SUBMITTED BY:

William Henze Jr.

W. Henze, Jr., Ph.D.

APPROVED BY:

N E Chatterton

N. E. Chatterton, Ph.D.
Manager, Research

TABLE OF CONTENTS

TABLE OF CONTENTS - Concluded

LIST OF ILLUSTRATIONS

LIST OF TABLES

1. INTRODUCTION

This report is a summary of the research in solar physics performed under Contract No. NAS8-31908 during the period from October 1976 through October 1977. All of the work involved data obtained by the Skylab-Apollo Telescope Mount (ATM) NASA-Marshall Space Flight Center/The Aerospace Corporation S-056 X-Ray Experiment during the Skylab mission. In certain areas, the work was performed jointly with colleagues from other institutions and, therefore, the appropriate sections of this report are preprints or reprints of jointly written papers.

Section 2 of this report consists of a description of the data obtained by the X-Ray Event Analyzer (X-REA), which was part of the S-056 experiment. The entire section formed a portion of the "Users' Guide to the Data Obtained by the Skylab/ATM NASA-Marshall Space Flight Center/ The Aerospace Corporation S-056 X-Ray Experiment", NASA Technical Memorandum X-73369. (A preliminary version of part of the remainder of the Users' Guide was included in the final report for Contract No. NAS8-26442 prepared in September 1976.)

Considerable effort was expended on the anlaysis of existing sensitometric data to establish the film calibration for the S-056 X-ray telescope. This work led to the report entitled "Film Calibration for the Skylab/ATM S-056 X-Ray Telescope", NASA Technical Memorandum 78122, which is presented in Section 3.

The analysis of the flare of 15 June 1973 was completed and two papers were prepared. The first, "Morphology and Physical Parameters of a Solar Flare" was published in The Astrophysical Journal, Vol. 216, pp. L79-L82, 1 September 1977; an altered version is reproduced in Section 4. The second has been submitted in revised form to Solar Physics. Only the section dealing with plasma diagnostics is presented in Section 5.

The X-REA observations of the solar soft X-ray flux were examined for evidence of periodic variations or oscillations. The results were included in a paper, which was submitted to Astronomy and Astrophysics. It is presented in Section 6.

Finally, the results of an investigation into whether deconvolution of the S-056 images is required are presented (Section 7). The images of the 5 September 1973 flare were used in the study.

2. X-RAY EVENT ANALYZER

(Extracted from "Users' Guide to the Data obtained by the Skylab/ATM NASA-Marshall Space Flight Center/The Aerospace Corporation S-056 X-Ray Experiment", NASA Technical Memorandum X-73369)

2.1 INSTRUMENT DESCRIPTION

The X-REA consisted of two proportional counters and associated electronics that monitored the soft X-ray flux from the entire Sun and provided a time history of the variation of emission from flares and other transient events. The X-REA operated continuously whenever the X-ray telescope was being used. In addition, the X-REA could be operated during unattended periods when the thermal shield door was open, as was the case during SL3. The X-REA is described in more detail by Underwood et al. (Ref. 2-1) and Wilson (Ref. 2-2).

The two detectors were conventional coaxial counters, gas-filled to 1 atm. The "soft" detector (usually called the aluminum counter) had an aluminum window supported by an 80% transmitting aluminum mesh and counted X-rays between the nominal wavelengths of 6.1 and 20 Å. The "hard" detector (usually called the beryllium counter) had a beryllium window and counted X-rays between the nominal wavelengths of 2.5 and 7.25 Å. Pulse-height analysis was used to separate the signals into various wavelength channels and thus provide coarse spectra. There were four channels for the aluminum counter and six channels for the beryllium counter. Both counters had integration times of 2.5 sec, and all channels were read out very 2.5 sec.

A four-position aperture wheel in front of each counter window increased the dynamic range of the X-REA. Each aperture was a factor of approximately four different in area from the next window. The apertures could be changed manually by the astronaut at the control panel or automatically (as usually used) when the counting rate reached a certain level.

The important X-REA properties are summarized in Table 2-1.

2.2 PROPORTIONAL COUNTER RESPONSE

The response of the various channels of the two proportional counters at the beginning of the Skylab mission to photons of different wavelengths is given in Tables 2-2 and 2-3 and is shown in Figures 2-1 and 2-2. The response is the probability of a count appearing in a channel for

TABLE 2-1. X-RAY EVENT ANALYZER PROPERTIES

			ALUMINUM COUNTER	BERYLLIUM COUNTER
Window Material and Thickness			0.25 mil (6.35 μm) Aluminum	10 mil (254 μm) Beryllium
Window Thickness (mg cm^{-2})			1.71	47
Gas Mixture			90% Argon 10% Methane	90% Xenon 10% Methane
Aperture Area (cm^2)	Aperture	1 2 3 4	2.45 (-3) 5.35 (-3) 2.04 (-2) 7.92 (-2)	2.04 (-2) 8.11 (-2) 3.22 (-1) 1.27 (0)
Nominal Channel Boundary Wavelengths at Start of Mission (Å)	Channel	1 2 3 4 5 6	16.0 to 20.0 12.0 to 16.0 8.0 to 12.0 6.1 to 8.0	6.00 to 7.25 5.50 to 6.00 5.00 to 5.50 4.50 to 5.00 3.75 to 4.50 2.50 to 3.75

TABLE 2-2. ALUMINUM COUNTER RESPONSE

WAVELENGTH (Å)	CHANNEL			
	1	2	3	4
4.5				9.30(-4)
5.0				4.50(-3)
5.5			2.60(-4)	9.35(-3)
6.0			6.61(-4)	1.06(-2)
6.5			9.91(-4)	7.41(-3)
7.0			9.60(-4)	3.51(-3)
7.5			6.45(-4)	1.21(-3)
7.95-			3.45(-4)	3.62(-4)
7.95+	1.50(-4)	5.03(-3)	2.10(-1)	2.20(-1)
8.0	1.67(-4)	5.45(-3)	2.15(-1)	2.12(-1)
8.5	4.31(-4)	1.12(-2)	2.54(-1)	1.35(-1)
9.0	9.48(-4)	1.97(-2)	2.65(-1)	7.68(-2)
9.5	1.82(-3)	3.02(-2)	2.51(-1)	3.95(-2)
10.0	3.10(-3)	4.13(-2)	2.19(-1)	1.86(-2)
10.5	4.76(-3)	5.12(-2)	1.80(-1)	8.08(-3)
11.0	6.68(-3)	5.83(-2)	1.40(-1)	3.27(-3)
11.5	8.66(-3)	6.15(-2)	1.03(-1)	1.24(-3)
12.0	1.04(-2)	6.06(-2)	7.28(-2)	4.41(-4)
12.5	1.18(-2)	5.61(-2)	4.93(-2)	1.49(-4)
13.0	1.25(-2)	4.93(-2)	3.21(-2)	
13.5	1.26(-2)	4.11(-2)	2.01(-2)	
14.0	1.21(-2)	3.27(-2)	1.21(-2)	
14.5	1.11(-2)	2.50(-2)	7.04(-3)	
15.0	9.66(-3)	1.83(-2)	3.96(-3)	
15.5	8.10(-3)	1.29(-2)	2.15(-3)	
16.0	6.52(-3)	8.82(-3)	1.13(-3)	
16.5	5.06(-3)	5.81(-3)	5.75(-4)	
17.0	3.78(-3)	3.70(-3)	2.83(-4)	
17.5	2.73(-3)	2.29(-3)	1.35(-4)	
18.0	1.91(-3)	1.37(-3)		
18.5	1.29(-3)	7.98(-4)		
19.0	8.45(-4)	4.51(-4)		
19.5	5.37(-4)	2.48(-4)		
20.0	3.31(-4)	1.33(-4)		
20.5	1.98(-4)			
21.0	1.15(-4)			

Note: Measurements given in (counts photon^{-1}).

TABLE 2-3. BERYLLIUM COUNTER RESPONSE

WAVELENGTH (Å)	CHANNEL					
	1	2	3	4	5	6
1.8						4.61(-4)
2.0						9.94(-3)
2.2						7.73(-2)
2.4						2.70(-1)
2.6					4.74(-4)	4.93(-1)
2.8					3.33(-3)	6.53(-1)
3.0				2.53(-4)	1.49(-2)	6.68(-1)
3.2			1.08(-4)	1.25(-3)	4.56(-2)	5.98(-1)
3.4			4.92(-4)	4.60(-3)	1.02(-1)	4.84(-1)
3.6		2.23(-4)	1.73(-3)	1.29(-2)	1.72(-1)	3.47(-1)
3.8	1.34(-4)	7.37(-4)	4.85(-3)	2.84(-2)	2.29(-1)	2.14(-1)
4.0	4.22(-4)	2.00(-3)	1.10(-2)	5.03(-2)	2.46(-1)	1.12(-1)
4.2	1.12(-3)	4.55(-3)	2.08(-2)	7.33(-2)	2.19(-1)	4.96(-2)
4.4	2.53(-3)	8.75(-3)	3.29(-2)	8.90(-2)	1.66(-1)	1.84(-2)
4.6	4.99(-3)	1.45(-2)	4.45(-2)	9.15(-2)	1.08(-1)	5.72(-3)
4.8	8.60(-3)	2.07(-2)	5.19(-2)	8.07(-2)	6.15(-2)	1.50(-3)
5.0	1.31(-2)	2.61(-2)	5.28(-2)	6.17(-2)	3.07(-2)	3.36(-4)
5.2	1.79(-2)	2.90(-2)	4.72(-2)	4.12(-2)	1.36(-2)	
5.4	2.20(-2)	2.87(-2)	3.74(-2)	2.43(-2)	5.32(-3)	
5.6	2.45(-2)	2.55(-2)	2.64(-2)	1.28(-2)	1.86(-3)	
5.8	2.48(-2)	2.04(-2)	1.67(-2)	5.98(-3)	5.79(-4)	
6.0	2.30(-2)	1.47(-2)	9.56(-3)	2.57(-3)	1.62(-4)	
6.2	1.96(-2)	9.69(-3)	4.96(-3)	9.57(-4)		
6.4	1.55(-2)	5.82(-3)	2.34(-3)	3.30(-4)		
6.6	1.14(-2)	3.20(-3)	1.01(-3)	1.03(-4)		
6.8	7.76(-3)	1.62(-3)	3.97(-4)			
7.0	4.95(-3)	7.53(-4)	1.44(-4)			
7.2	2.95(-3)	3.24(-4)				
7.4	1.65(-3)	1.29(-4)				
7.6	8.71(-4)					
7.8	4.31(-4)					
8.0	2.01(-4)					

Note: Measurements given in (counts photon^{-1}).

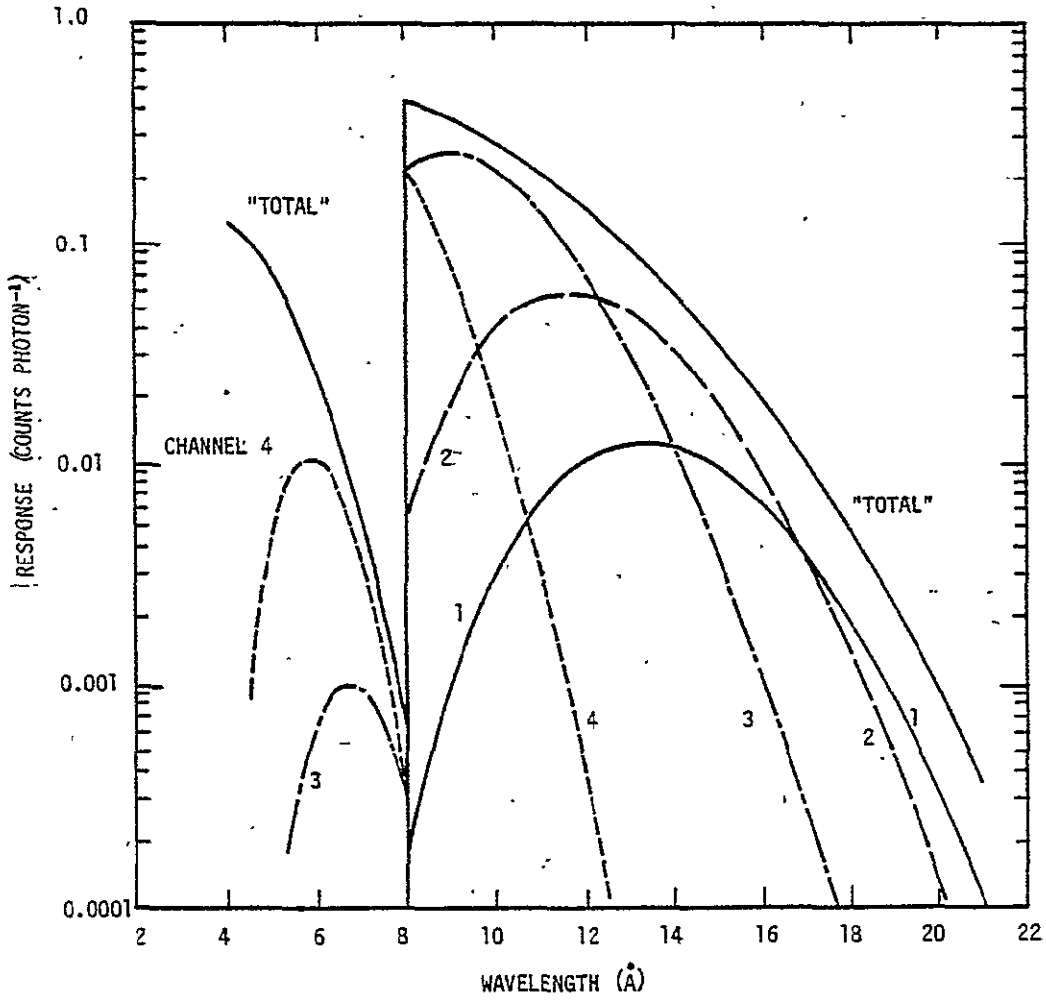

FIGURE 2-1. ALUMINUM COUNTER RESPONSE

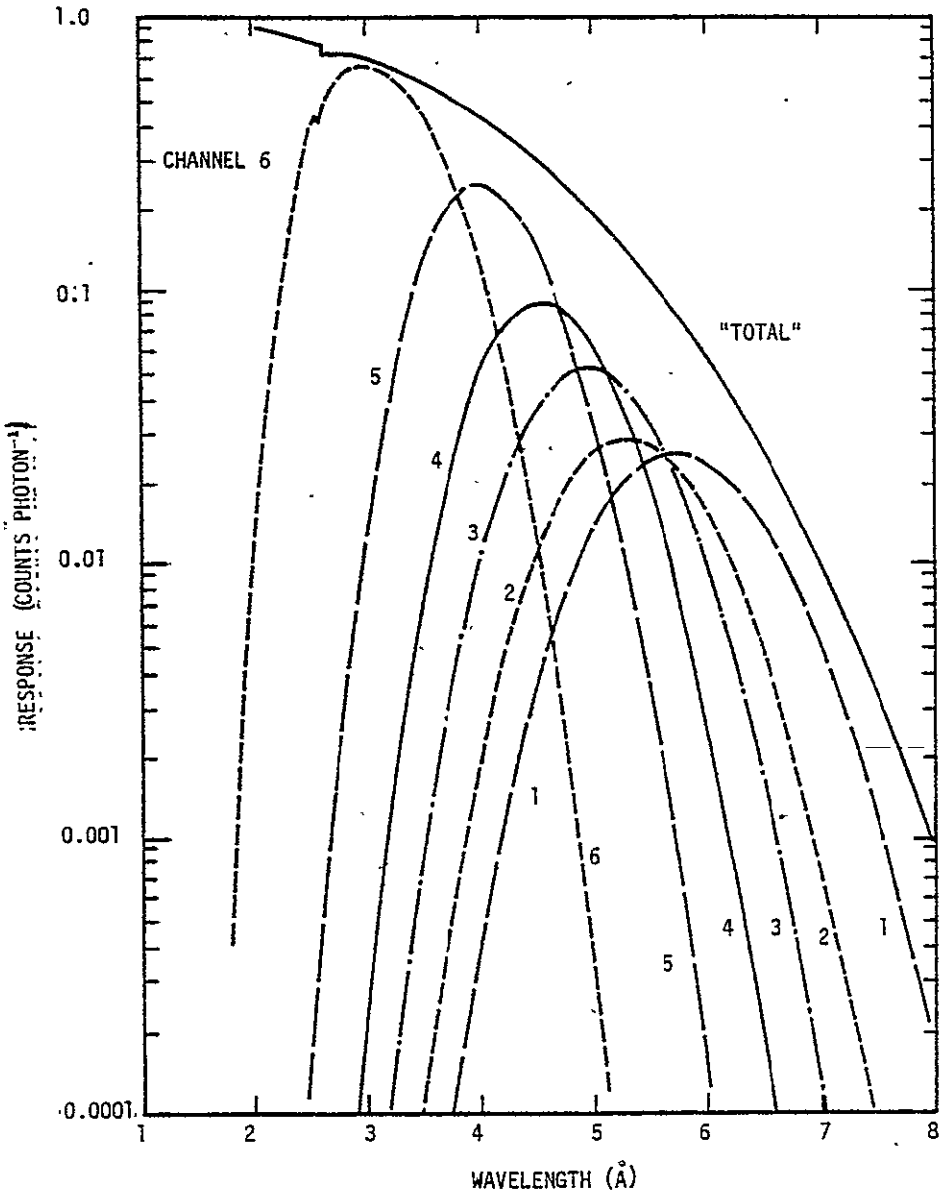

FIGURE 2-2. BERYLLIUM COUNTER RESPONSE

each photon as a function of wavelength of the photon. The response of each channel extends beyond the wavelength boundaries given in Table 2-1 because of the finite energy-resolution width inherent in proportional counters.

Also presented in Figures 2-1 and 2-2 is the "total" counter efficiency, the product of the window transmission and the absorption efficiency of the gas. (The "total" response is greater than the sum of the responses of the individual channels because the pulse-height analyzers excluded photons whose apparent energies were outside the extreme limits of the highest and lowest channels.) As can be seen, the strong wavelength dependence of the efficiency sometimes dominates the variation of the response so that the peak of the response function for a particular channel can occur outside its nominal wavelength boundaries.

At the start of the mission, the counters exhibited excessively large count rates in the low-energy, long-wavelength channels. The cause of the low-energy excess is not yet understood, and those channels should be avoided or used with caution.

The performance of the counters degraded during the mission. The gain changed so that the wavelength boundaries of the channels and the counter efficiency also changed. Caution is advised in the use of the absolute values of the count rates and the channel ratios for all channels after the first manned mission (SL2).

2.3 X-REA OBSERVATIONS

The scientific data from the X-REA are included in the 565 rolls of microfilm records submitted to the NSSDC that also contain the current, temperature, and discrete event measurements. Figure 2-3 shows the format of the records. The basic data consist of the counts accumulated for 2.5 sec for each channel as a function of time (at 2.5-sec intervals). Also presented are the sums of the counts in all channels for each counter and the aperture positions. An asterisk following the ground station

XREA SCIENTIFIC DATA K0113-056 BATCH 153-3

	GMT	APER POS.	ALUMINIUM 1	2	3	4	TOTALS AL	BE	BERYLLIUM 1	2	3	4	5	6	APER POS.	STATION
(a)	153:14:53:39.6	1	0	7	0	0	7	23315	401	0	0	12080	10834	0	4	HAW*
	153:14:53:42.1	1	0	7	0	0	7	23315	401	0	0	12080	10834	0	4	HAW*
	153:14:53:44.6	1	0	7	0	0	7	23315	401	0	0	12080	10834	0	4	HAW*
	153:14:53:47.1	1	0	7	0	0	7	23315	401	0	0	12080	10834	0	4	HAW*
	153:14:53:49.6	1	0	7	0	0	7	23315	401	0	0	12080	10834	0	4	HAW*
	153:14:53:52.1	1	0	7	0	0	7	23315	401	0	0	12080	10834	0	4	HAW*
(b)	153:14:59:54.6	1	2212	2221	2217	2216	8866	8950	1492	1481	1416	1565	1502	1494	1	HAW
	153:14:59:57.1	1	2211	2222	2216	2216	8865	8952	1492	1483	1431	1546	1505	1495	1	HAW
	153:14:59:59.6	1	2387	2180	2025	2217	8809	8952	1492	1482	1436	1547	1502	1493	1	HAW
(c)	153:15: 0:27.1	4	0	0	0	1	1	10	1	2	1	1	1	4	4	HAW
	153:15: 0:29.6	4	0	0	3	2	5	11	4	1	0	1	1	4	4	HAW
	153:15: 0:32.1	4	4	1	1	1	7	13	1	1	2	0	2	7	4	HAW
	153:15: 0:34.6	4	0	0	1	0	1	11	3	0	0	2	3	3	4	HAW
	153:15: 0:37.1	4	2	1	1	3	7	9	2	0	0	1	0	6	4	CRO*
	153:15: 0:39.6	4	0	1	2	1	4	6	1	1	0	0	0	4	4	CRO*
	153:15: 0:42.1	4	1	0	2	1	4	9	2	0	0	2	0	5	4	CRO*
	153:15: 0:44.6	4	0	0	2	2	4	6	3	0	0	0	0	3	4	CRO*
(d)	153:15: 1:24.6	4	70	451	557	50	1128	264	113	47	38	33	21	12	4	CRO*
	153:15: 1:27.1	4	283	1140	1312	81	2816	445	201	80	85	46	29	9	4	CRO*
	153:15: 1:29.6	3	476	1375	1926	54	3831	513	242	93	70	62	33	13	4	CRO*
	153:15: 1:32.1	3	216	669	1606	36	2527	554	282	100	86	49	30	7	4	CRO*
	153:15: 1:34.6	3	342	934	797	25	2098	594	318	90	95	50	35	6	4	CRO*
	153:15: 1:37.1	3	510	1121	995	30	2656	658	351	116	78	66	32	15	4	CRO*
	153:15: 1:39.6	3	606	1431	1013	22	3152	648	347	107	94	64	33	3	4	CRO*
	153:15: 1:42.1	3	827	1510	1090	27	3454	671	371	120	87	49	32	12	4	CRO*
	153:15: 1:44.6	3	1000	1758	1167	20	3945	690	391	101	82	68	39	9	4	CRO*
	153:15: 1:47.1	3	1073	1800	1247	21	4141	684	374	119	90	54	39	8	4	CRO*
	153:15: 1:49.6	3	1111	1965	1223	33	4332	679	365	113	85	60	43	13	4	CRO*
	153:15: 1:52.1	3	1274	1994	1266	25	4559	687	371	114	95	58	39	10	4	CRO*
	153:15: 1:54.6	3	1306	2041	1284	21	4652	689	369	123	92	64	31	10	4	CRO*
	153:15: 1:57.1	3	1390	2204	1318	25	4927	690	374	123	101	47	31	14	4	CRO*
	153:15: 1:59.6	3	1384	2142	1336	28	4890	721	403	125	85	60	35	13	4	CRO*
	153:15: 2: 2.1	3	1352	2184	1357	27	4920	689	379	116	97	51	37	9	4	CRO*
	153:15: 2: 4.6	3	1455	2214	1353	32	5054	698	376	133	87	58	33	11	4	CRO*
	153:15: 2: 7.1	2	972	1382	1391	20	3765	715	400	107	100	65	34	9	4	CRO*
	153:15: 2: 9.6	2	466	767	784	13	2030	690	389	125	81	60	27	8	4	CRO*
	153:15: 2:12.1	2	491	790	517	13	1811	730	401	139	101	58	35	4	4	CRO*
	153:15: 2:14.6	2	433	804	526	13	1776	703	416	108	85	59	31	4	4	CRO*

NOTE: The four sets of data illustrate (a) counters off, (b) calibration mode, (c) background counts with counters on and thermal shield door closed, (d) solar observations with counters on and door open. The solar observations also illustrate aperture changes caused by an increasing count rate during a sunrise.

FIGURE 2-3. EXAMPLE OF PRINTOUTS OF S-056 X-REA DATA ON MICROFILM

abbreviation indicates that the data came from the recorder. (The X-REA data were both telemetered in real time when Skylab was in range of a ground station and recorded on board for later transmissions; however, this information is normally not important to users.)

The X-REA data are also available at the experimenters' institutions on magnetic tape and on printouts.

Essentially, the data recorded in the microfilm records are "raw" in that no background counts have been removed, nor has any correction factor been applied to the data to adjust it for degradation of the counters with time. X-REA data immediately following an aperture position change should be discarded because the aperture wheel may have changed during the 2.5-sec accumulation. Sometimes, two lines of readout must be discarded, apparently because of noise spikes associated with the aperture change. Also, on occasion, the telemetry record indicates an incorrect aperture position for the counters, which is apparant only when data from both counters prior to, during, and following the period of interest are compared. The spurious aperture indication has been particularly noted in data from the SL3 mission.

Typical X-REA data fall into four categories, as shown in Figure 2-3. First, when the counters are off, the readings are asterisks, zeros, or constant numbers (generally in only one or two channels). Second, when the X-REA was placed in the "calibration mode", a predetermined number appeared in all channels and total counts columns. The calibration signal verified the operation of the counter electronics only. No calibration source to verify the counter gas response was employed in the instrument. Third, when the counters were on with the thermal shield door closed, the readings indicate background counts. These counts increased during passages through the South Atlantic Anomaly (SAA) and the "horns" of the Van Allen radiation belts. Finally, when the counters were on and the door was open, the readings reflect the counts resulting from X-rays from the Sun. Again, these solar counting rates were occasionally contaminated with high background counts due to the SAA and the "horns".

2.4 QUANTITATIVE ANALYSIS OF X-REA OBSERVATIONS

The interpretation of the counts described in Section 2.3 in terms of the X-ray flux emitted by the Sun involves the following procedure.

The observed counts, ψ_n, as given on the microfilm, where n denotes the channel, were accumulated for a time, t (equal to 2.5 sec), and with an aperture also indicated on the microfilm. Therefore, ψ_n should be divided by t and then divided by the aperture area, A, to obtain the solar photon flux at the detector integrated over the response of the channel; i.e.,

$$\int \eta_n(\lambda)\ \phi_\lambda(\lambda)\ d\lambda = \frac{\psi_n}{At} \quad \text{(in photons cm}^{-2}\ \text{sec}^{-1}\text{)} \ ,$$

where $\eta_n(\lambda)$ is the probability of a count appearing in channel n per photon at wavelength λ and $\phi\lambda(\lambda)$ is the solar photon flux incident on the detector (in photons cm^{-2} sec^{-1} $\mathring{A}^{-1}$). The aperture area is given in Table 2-1, and η_n is given in Tables 2-2 and 2-3 and Figures 2-1 and 2-2. The solar flux is related to the intensity, I_λ, by

$$\phi_\lambda = \int \frac{I_\lambda}{h\nu}\ d\Omega \ ,$$

where $h\nu$ is the energy per photon and the integral over solid angle Ω covers the field of view (in this case, the entire Sun as seen from the observing instrument).

As before, the further interpretation of the data requires the introduction of assumed spectra. The spectra, usually theoretical spectra for an optically thin plasma of coronal composition and temperature, are multiplied by η_n and integrated over the wavelength band. The results are then compared with the observations. Wilson (Ref. 2-2) has given an example of such an analysis.

In general, extreme caution is advised in the quantitative interpretation of the X-REA observations. Prospective users are urged to contact the S-056 data analysis groups before performing any quantitative work.

REFERENCES - SECTION 2

2-1. J. H. Underwood, J. E. Milligan, A. C. deLoach, and R. B. Hoover, "The S-056 X-Ray Telescope Experiment on the Skylab-Apollo Telescope Mount", Applied Optics, Vol. 16, pp. 858-869, 1977

2-2. R. M. Wilson, "The Skylab ATM/S-056 X-Ray Event Analyzer: Instrument Description, Parameter Determination, and Analysis Example (15 June 1973 1B/M3 Flare)", Marshall Space Flight Center, NASA TM X-73332, 1976

3. FILM CALIBRATION FOR THE SKYLAB/ATM S-056 X-RAY TELESCOPE

(Reproduced in its entirety from NASA Technical Memorandum 78122)

Authors

W. Henze, Jr.
Teledyne Brown Engineering
Huntsville, Alabama

R. M. Broussard
Aerospace Corporation
El Segundo, California

J. H. Underwood
Institute of Plasma Research
Stanford University

J. P. McGuire
E. J. Reichmann
Space Sciences Laboratory
NASA - Marshall Space Flight Center

J. B. Smith, Jr.
NOAA/SEL; Presently Located at Marshall
Space Flight Center

3.1 INTRODUCTION

The purpose of this report is to summarize the sensitometry and film calibration effort for the NASA-MSFC/The Aerospace Corporation Skylab/ATM S-056 X-Ray Telescope (Ref. 3-1). It includes descriptions of the films used, the sensitometry performed, the characteristic curves for the flight film, and the use of copy films. A brief summary of the history of the overall S-056 film calibration effort is given in this introduction.

Five rolls (or loads) of 35-mm film were exposed by S-056 during the three manned Skylab missions, four of black-and white film (SO-212) and one of color-reversal film (SO-242). These rolls of film are referred to as flight film, originals, or first-generation film. Table 3-1 shows that one roll of black-and-white film was used on the first manned mission, SL2; two rolls were used on SL3; and one roll of black-and-white and one roll of color film were used on SL4. (Note that Load 5, the color film, was exposed before Load 4.)

Film tests and calibration were conducted by Sperry Support Services (Sperry Rand Corporation) and The Aerospace Corporation. As part of the S-056 hardware development program, a film testing and calibration facility was constructed at MSFC. This facility was used by Sperry to perform preflight and postflight sensitometry on the flight film as well as other film tests. Early in 1973, Aerospace became involved in the S-056 program and was directed to undertake a parallel sensitometric effort. In addition to general tests on the film, Aerospace made postflight calibration exposures on the flight film.

Section 3-2 describes the apparatus and procedures used by Aerospace and Sperry. Section 3-3 describes the two types of flight films used, including the results of some of the tests made thereon. The sensitometry and processing of the flight films are described in Section 3-4. The resulting characteristic curves are given in Section 3-5 together with a description of the data reduction required to obtain the curves. Section 3-6 covers the use of various copies that have been made of the flight film, including a description of the properties of the different types of copy films.

TABLE 3-1. S-056 FILM USAGE

MISSION	LOAD	FILM TYPE	DATES	DAY OF YEAR	FRAMES USED
SL2	1	SO-212 (B&W)	29 May 1973 - 18 Jun 1973	149 to 169	3998
SL3	2	SO-212 (B&W)	07 Aug 1973 - 24 Aug 1973	219 to 236	5653
	3	SO-212 (B&W)	24 Aug 1973 - 21 Sep 1973	236 to 264	5797
SL4	5	SO-242 (Color)	26 Nov 1973 - 25 Dec 1973	330 to 359	5029
	4	SO-212 (B&W)	26 Dec 1973 - 03 Feb 1974	360 to 34	6713
				TOTAL	27 190

3.2 SENSITOMETRY APPARATUS AND PROCEDURES

3.2.1 Sperry/MSFC

An X-ray sensitometer chamber, designed to place X-ray sensitometry on the S-056 film, was placed in operation at MSFC by Sperry in November 1972. A schematic of that facility is shown in Figure 3-1. The source of X-rays was a Henke tube. There were two other Henke tubes in the chamber as backups. The X-rays went through an exact duplicate mechanism as the camera on S-056, minus the optics. The filters used were also exact duplicates of the flight hardware.

A proportional counter, called the monitor counter, was placed just forward of the camera system, with its own set of duplicate flight filters, to monitor the X-ray source. Another counter, called the spectral proportional counter, was capable of being moved behind the camera filter wheel mechanism to measure the X-ray flux at the film plane. In this position, the counter took the place of the film. An Fe55 source was used as a calibration source for the pulse-height analyzer associated with the spectral proportional counter. The Fe55 source emitted Mn Kα X-rays at an energy of 5.9 keV (2.1 Å).

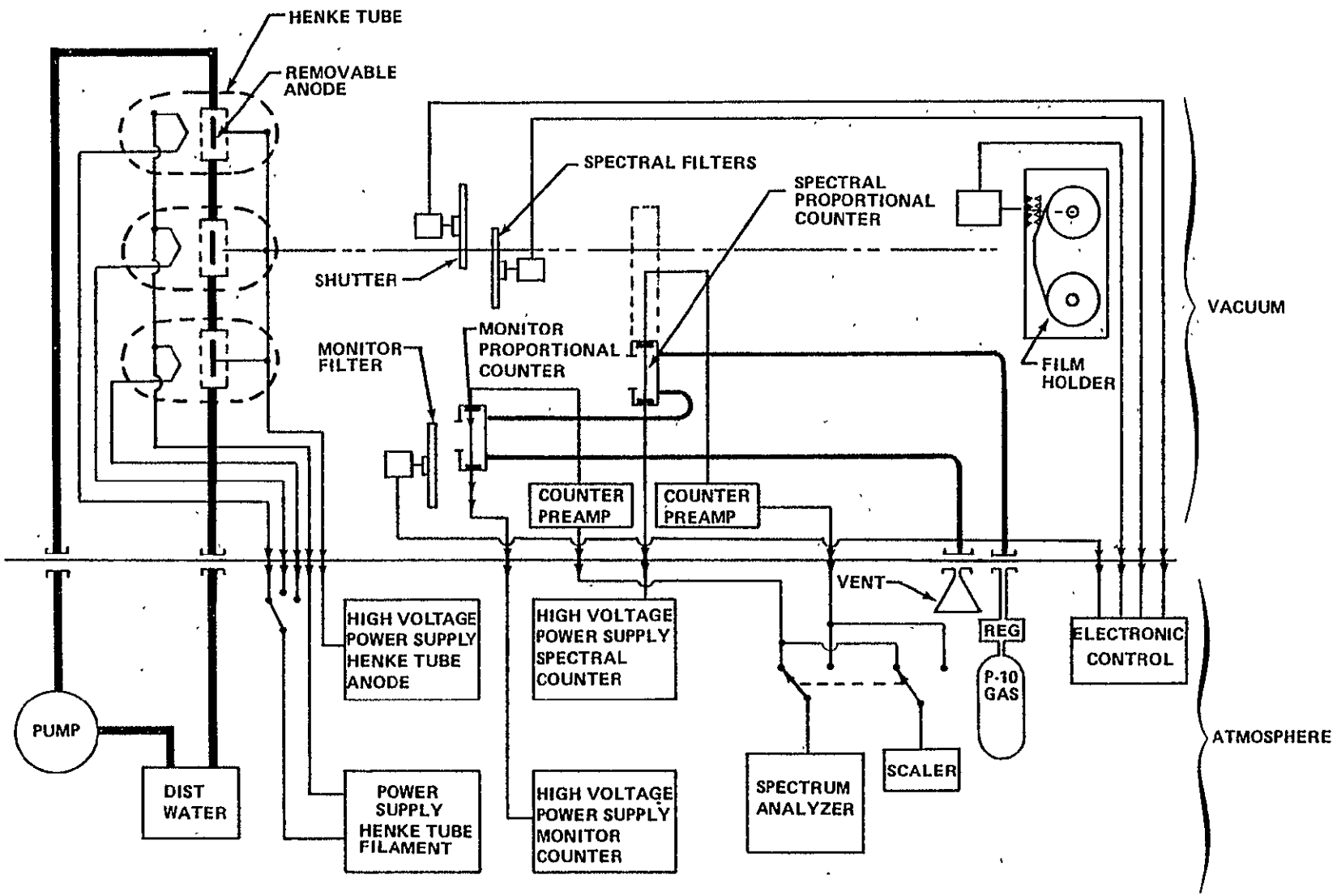

FIGURE 3-1. SCHEMATIC DIAGRAM OF SPERRY/MSFC X-RAY SENSITOMETRY CHAMBER

Various anode materials were used with the Henke tubes to produce X-rays at different wavelengths. The three primary lines used were Al Kα (8.34 Å), Cu Lα (13.3 Å), and Ti Lα (27.4 Å). The Henke tubes also emitted continuous radiation so that the X-rays produced were not monochromatic but contained both line and continuum components. The filters used then determined the final spectral distribution of the X-rays incident on the film.

Exposure times for the various steps of a set of sensitometer exposures ranged from 1 sec to 4 hr 33 min and 4 sec. During an exposure sequence, proportional counter readings were usually taken with the spectral counter before and after the sequence and sometimes between some of the individual exposures. Occasionally the monitor counter was used to take readings at the same time that individual exposures were being made.

3.2.2 Aerospace

The general film tests and sensitometric effort were completed at Aerospace on the apparatus shown in Figure 3-2.

The film under test was contained in the electrically driven Nikon camera. The lens of this camera was replaced by a tube whose outer end was covered by a filter to transmit X-rays of the desired wavelength and exclude visible light. The X-ray tube employed was specifically designed for that purpose. It was evacuated by a separate Vacion pumping system and isolated from the main tank by a very thin plastic window. In this way, contamination of the target by diffusion pump oil was held to a minimum, so that the characteristic lines of the target element were efficiently produced. Various target/filter combinations ensured that radiation of the desired wavelength reached the film. A proportional counter was used to detect the X-ray flux. For any exposure sequence, the counter was fitted with a window of exactly the same material as the filter covering the film. Pulse height analysis of the proportional counter pulses was employed to determine if the radiation reaching the film was of the correct wavelength.

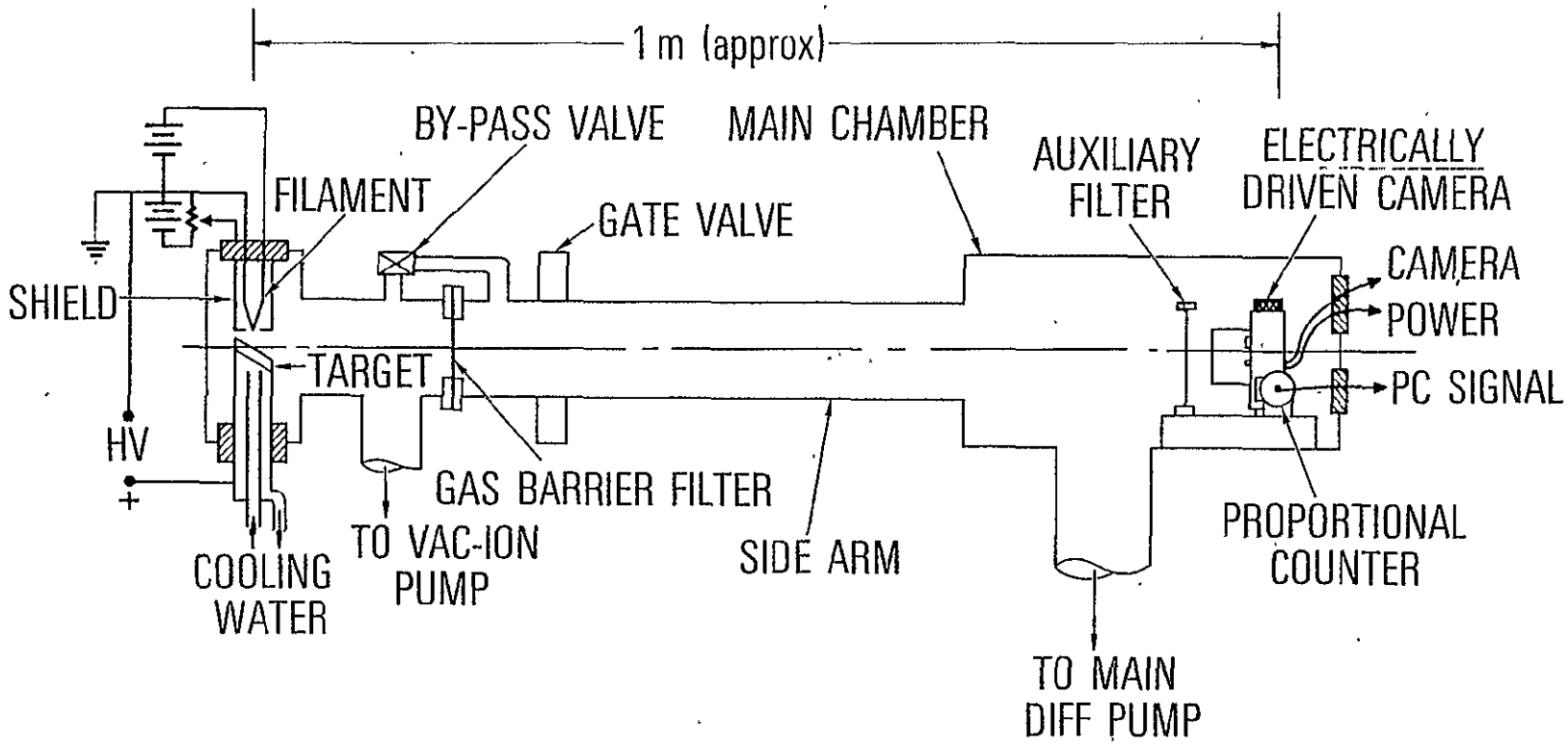

FIGURE 3-2. SCHEMATIC DIAGRAM OF AEROSPACE X-RAY SENSITOMETRY CHAMBER

The counter operated during the whole of each exposure, and the total counts were recorded. The number of photons reaching the film was then determined through a calculation based on the geometry. This required a knowledge of the counter aperture and distances of counter and film from the source. The source was assumed to be a point source so that the inverse square law applied.

In a typical sensitometric run (for example, those made for the postflight X-ray calibration strips), the exposures received by the film ranged between 5×10^6 and 1×10^{10} photons/cm^2. The flight sensitometry strips were exposed to X-rays of wavelengths 8.34 Å (Al K) and 13.3 Å (Cu L). Further tests on nonflight film were made at the wavelengths 5.4 Å (Mo L), 9.89 Å (Mg K), 16.0 Å (Co L), 27.4 Å (Ti L), and 44.6 Å (C K).

3.3 PROPERTIES OF FLIGHT FILMS

3.3.1 SO-212 Film

The primary film used with the S-056 telescope was a black-and-white film, Kodak Type SO-212; four rolls were exposed during the three manned missions. The SO-212 film, developed by Kodak especially for the X-ray telescopes on Skylab, had a Panatomic-X emulsion but without a protective gelatin overcoat and with a Rem-Jet antistatic backing. This same film, in a 70-mm format, was used in the American Science and Engineering (AS&E) S-054 X-Ray Spectrographic Telescope on Skylab (Ref. 3-2). This section summarizes the history of the development of SO-212 film and then describes some of its properties.

Kodak Panatomic-X Aerial Film 3400 (Ref. 3-3) possessed many of the characteristics of resolution, contrast, and sensitivity desired by the Skylab X-ray experimenters. A special version of this film, designated SO-114, was produced by Kodak without the normal protective gelatin overcoat. This film was tested by Sperry (Ref. 3-4) and by AS&E (Ref. 3-2). The overcoat was omitted to eliminate absorption of the incident X-rays by the gelatin and thus increase the speed of the film. However, tests in a vacuum chamber indicated that the extreme

drying of the film in the vacuum led to fogging of the film by static electrical discharges (Ref. 4-4). Two measures were taken to alleviate the problem of the discharges. First, a moisture source (potassium thiocyanate salt pads) was added to each magazine. Second, a Rem-Jet antistatic carbon backing was provided on the film which then was designated SO-212. The final film thus consisted of the emulsion mounted on Estar Thin Base with the Rem-Jet backing.

The X-ray response of the SO-212 film was extensively studied by Sperry, Aerospace, and AS&E. Tests conducted at Aerospace for the specific wavelengths mentioned in Section 3.2.2 indicated that the film response for wavelengths between 5.4 and 16 Å was identical when the exposures were plotted as a photon flux (in photons cm^{-2}) (Ref. 3-5). From this study, it was concluded that the film acted as a photon detector. This result was used in subsequent S-056 analyses. In independent studies on the S-054 film, AS&E related the film density to the X-ray energy deposited on the film (in erg cm^{-2}) (Ref. 3-6). They found some variation of the film response with wavelength. The difference in the response of the S-056 and S-054 films, especially in the shoulder portion of the characteristic curve, may be caused by the difference in processing of the two films (Ref. 3-6). Work by Sperry at 8.3 and 27 Å suggested different values of gamma (contrast) at the two wavelengths; the value of gamma appeared to be lower at the longer wavelength.

Although study of the nature of the film response is continuing, the quantitative analyses of the S-056 films have thus far been based on the assumption that the film behaved as a photon detector with the same sensitivity for photons at all wavelengths. If the film acted as an energy detector at the longer wavelengths or showed a variation of gamma with wavelength, the results of the analyses would be changed somewhat. However, only those images taken through one of the S-056 filters (Filter No. 3) would be significantly affected and, even then, only for low temperature solar features. The remaining four X-ray filters, though broadband (Ref. 3-1), cover a wavelength range that is sufficiently narrow so that the analyses should remain reliable.

3.3.2 SO-242 Film

Although the black-and-white film, SO-212, was the primary film used with the S-056 telescope, one roll of color film, Kodak Type SO-242, was exposed on the third manned Skylab mission (SL4). The SO-242 film is an aerial color-reversal film (Refs. 3-3 and 3-7) with slightly better resolution but slower speed than SO-212. The reason for using the color film was the realization that the color (visible light color) of an X-ray image depends on the spectral distribution of the X-rays incident on the film. This effect, discussed further later, is caused by the wavelength variation of the X-ray absorption coefficient of the emulsion. In principle, one should be able to infer information about the X-ray spectral distribution from color densitometry (or simple densitometry of black-and-white color-separation copies). In practice, the lack of good absolute sensitometry at a number of well-defined wavelengths combined with the complicated nature of the solar spectrum which must be folded into the film sensitivity curves for the different colors has made it difficult to utilize the color property of the film.

The overall properties of the SO-242 film and some of its test results have been described by Clune et al. (Ref. 3-8). Their paper forms the basis for much of the following discussion.

The film consists of 11 gelatin layers on a polyester base (Estar Thin Base) with a thin clear-gel backing. The gelatin layers consist of a protective overcoat, ultraviolet absorbing layer, green-sensitive emulsion, dye-absorbing layer, red-sensitive emulsion, dye-absorbing layer, blue-sensitive emulsion, three gelatin separation layers, and an antihalation coat. Because of absorption by the gelatin, all layers do not receive the same irradiance; i.e., the surface layers receive a higher exposure than the deeper layers. The major contributors to the absorption are carbon, oxygen, and nitrogen, with the absorption coefficient varying approximately as the cube of the wavelength except for abrupt decreases at absorption edges. The edges in the relevant spectral region are the K edges of C (43.7 Å), O (23.3 Å), and N (30.9 Å);

however, even these edges would be significant only for S-056 Filter No. 3 with its long-wavelength window, and Filter No. 3 had developed a light leak and was generally unusable during the time that the SO-242 film (Load 5) was being exposed on Skylab. Thus, in the important spectral region from 6 to 18 Å, the absorption coefficient of the gelatin increases with wavelength so that the short wavelength photons are more likely to penetrate to the blue-sensitive emulsion layer. Therefore, one would expect that a hot solar event such as a flare with a harder spectrum would produce a bluer image than an active region with a cooler, softer spectrum.

Clune et al. (Ref. 3-8) have presented data that verify the above qualitative discussion. They give H&D curves at two median wavelengths, 14.3 Å and 7.9 Å, where the blue, green, and red densities are plotted against the logarithm of the exposure. In the 14.3-Å case, the blue and green density curves are almost identical. At 7.9 Å, the blue density curve is approximately 0.8 in log exposure to the left of the green curve, thus showing a bluer image. These results and tests at other wavelengths were made with the MSFC/Sperry X-ray sensitometer. Because of the difficulty in getting absolute experimental data at more nearly monochromatic wavelengths that would then have to be folded into theoretical spectra, the calibration curves to be presented in Section 3.5 are for visible, white-light densities so that the color effects have been ignored. Thus far, the color film has been treated the same as black-and-white film. However, the possibility of utilizing the color properties of the color film in the future has not been eliminated.

3.4 FLIGHT FILM SENSITOMETRY AND PROCESSING

In this section, the various types of sensitometry performed on the flight films are described and the format and positions of the sensitometric sets are indicated. The processing of the flight films is also summarized.

3.4.1 Sensitometry

For calibration of the actual flight films, sets of sensitometry were placed on the films before and after each mission. Usually, the preflight sets were spliced onto the beginning (known as the "heads") of each roll, while the postflight sets were sliced onto the end (known as the "tails") of the roll. Tables 3-2 through 3-6 identify each set for each load, showing the order in which they are present and giving additional information concerning each set.

As can be seen from the tables, the films contain several different types of sensitometry. In addition to the X-ray sensitometry performed by Sperry and Aerospace, there are visible light (Vis) and ultraviolet (UV) sets provided by Sperry and photographic white-light (WL) wedges was to monitor changes in film properties as a result of exposure to the space environment. The appearance of a typical step for each type of sensitometry is shown in Figure 3-3. Some second- or third-generation copies may also have additional photographic wedges at the very beginning and end; these were provided to monitor the constancy of the duplicating process. The numbering of the X-ray sets is based on the numbers assigned or used by Sperry and Aerospace. Numbers for other sets, if given at all, were assigned simply for convenience.

The preflight X-ray sensitometry was performed only by Sperry and is available for Loads 1 through 4. No preflight sensitometry was spliced onto Load 5, the color film. However, two test sets were exposed on the color film as part of a group of environmental simulation test samples. The test sets were made by Sperry after the SL4 mission had been launched; therefore, the samples of film used did not fly on Skylab although they were stored and then spliced onto and processed with the Load 5 flight film.

Sperry and Aerospace performed postflight sensitometry for all five loads. However, the Aerospace sensitometry on Load 3 is not usable because of overlapping exposures, apparently caused by film advance problems. In addition, some of the Sperry sets, especially postflight on Load 2, also had overlapping steps and were not completely usable.

TABLE 3-2. LOAD 1, IDENTIFICATION OF SENSITOMETRY SETS

ORIGIN OF SENSITOMETRY SET	TYPE OF SENSITOMETRY	PRE OR POST FLIGHT	SOURCE OR λ(A)	SET NO.	END OF SET WITH HIGH EXPOSURES	NUMBER OF STEPS (INTENDED OR ACTUAL)	REMARKS, STEP SIZE, OTHER FEATURES ON FILM
↑ HEADS END							
Sperry	X-Ray	Post	Ti	109	H	21	Each step 5/16-in. wide (along film), 1 1/2 in. from center to center
Sperry	X-Ray	Post	Ti	108	H	22	Same as Set 109
Sperry	X-Ray	Post	Al	107	H	21	Same as Set 109 ◁ Trapezoidal piece of tape on flight film
Sperry	X-Ray	Post	Al	106	H	21	Same as Set 109 ▷ Trapezoidal piece of tape on flight film 1 1/4 in. wide gate (highly exposed)
Sperry	Visible	Post	6400		T	21	Each step 3/8 to 1/2 in. wide, 5/8 in. from center to center
Sperry	Visible	Post	5200		T	21	Same as λ6400
Sperry	Visible	Post	4000		T	21	Same as λ6400 1-in. wide gate (highly exposed)
Sperry	UV	Post	2600		T	21	Same as λ6400
Aerospace	X-Ray	Post	Al		T	28	
Aerospace	X-Ray	Post	Cu		T	15	15 3/4-in. highly exposed section
JSC	Photo	Pre	WL	1	T		
JSC	Photo	Pre	WL	2	T		Tick mark tenth step from Tails
Sperry	UV	Pre	2600		H	21	Each step 3/8 to 7/16 in. wide, 5/8 in. from center to center
Sperry	Visible	Pre	4000		H	21	Same as λ2600
Sperry	Visible	Pre	5200		H	21	Same as λ2600
Sperry	Visible	Pre	6400		H	21	Same as λ2600
Sperry	X-Ray	Pre	Al	1	T	27	Each step 5/16 in. wide, 1 1/2 in. from center to center; some overlapping steps
Sperry	X-Ray	Pre	Ti	2	T	24	Same step size and spacing as Set 1
Sperry	X-Ray	Pre	Al	3	T	24	Same as Set 2
Sperry	X-Ray	Pre	Ti	4	T	23	Same as Set 2
SOLAR IMAGES							
JSC	Photo	Post	WL	3	T		
JSC	Photo	Post	WL	4	T		
↓ TAILS END							

H = Heads, T = Tails; WL = White Light; UV = Ultraviolet Light; Photo = Photographic

TABLE 3-3. LOAD 2, IDENTIFICATION OF SENSITOMETRY SETS

ORIGIN OF SENSITOMETRY SET	TYPE OF SENSITOMETRY	PRE OR POST FLIGHT	SOURCE OR λ(A)	SET NO.	END OF SET WITH HIGH EXPOSURES	NUMBER OF STEPS (INTENDED OR ACTUAL)	REMARKS, STEP SIZE, OTHER FEATURES ON FILM
↑ HEADS END							
Sperry	UV	Pre	2600		H	21	Each step 3/8 to 7/16 in. wide, 5/8 in. from center to center
							1 in. wide gate (highly exposed)
Sperry	Visible	Pre	4000		H	21	Same as λ2600
Sperry	Visible	Pre	5200		H	21	Same as λ2600
Sperry	Visible	Pre	6400		H	21	Same as λ2600
							1 3/8 in. wide gate (?), 1 1/2-in.- wide gate (?)
Sperry	X-Ray	Pre	Al	047-I	T	21	Each step 5/16 in. wide, 1 1/2 in. from center to center
Sperry	X-Ray	Pre	Al	047-II	T	21	Same as Set 047-I
							6-in. highly exposed section
JSC	Photo	Pre	WL	1	T		
JSC	Photo	Pre	WL	2	T		
SOLAR IMAGES							
JSC	Photo	Post	WL	3	T		
JSC	Photo	Post	WL	4	T		
							1/2-in. splice, 1 in. wide gate
Sperry	Visible	Post	6400		T	21	Each step 3/8 to 1/2 in. wide, 5/8 in. from center to center
Sperry	Visible	Post	5200		T	21	Same as λ6400
Sperry	Visible	Post	4000		T	21	Same as λ6400
Sperry						1	Step is centered in 1 in. wide, lightly exposed section (gate ?)
Sperry	UV	Post	2600		T	21	Same as λ6400
							1 in. wide gate, ~3 1/2 in. highly exposed section
Sperry	X-Ray	Post	Ti	165			Messed up, steps superimposed
Sperry	X-Ray	Post	Al	164	H	22	Many touching or overlapping steps, close to Set 165
Sperry	X-Ray	Post	Ti	163	H	21	Each step 5/16 in. wide, 19/32 in. normal center to center
Sperry	X-Ray	Post	Al	162	H	21	Same as Set 163
							12 in. long, ~10 1/2 in. long highly exposed sections
Aerospace	X-Ray	Post			H	2	
Aerospace	X-Ray	Post	Al		H	17	
Aerospace	X-Ray	Post				1	Very-faint
Aerospace	X-Ray	Post			H	17	
Aerospace	X-Ray	Post			T	2	
↓ TAILS END							

TABLE 3-4. LOAD 3, IDENTIFICATION OF SENSITOMETRY SETS

ORIGIN OF SENSITOMETRY SET	TYPE OF SENSITOMETRY	PRE OR POST FLIGHT	SOURCE OR λ(A)	SET NO.	END OF SET WITH HIGH EXPOSURES	NUMBER OF STEPS (INTENDED OR ACTUAL)	REMARKS, STEP SIZE, OTHER FEATURES ON FILM
↑ HEADS END							
Sperry	UV	Pre	2600		H	21	Each step 3/8 to 1/16 in. wide, 5/8 in. from center to center
							1 in. wide gate (highly exposed)
Sperry	Visible	Pre	4000		H	21	Same as λ2600
Sperry	Visible	Pre	5200		H	21	Same as λ2600
Sperry	Visible	Pre	6400		H	21	Same as λ2600
							1 1/2 in. wide gate (?)
Sperry	X-Ray	Pre	Al	048-I	T	22	Each step 5/16 in. wide, 1 1/2 in. from center to center
Sperry	X-Ray	Pre	Al	048-II	T	20	Same as Set 048-I
							~2 1/4 in. highly exposed section, 1/2 in. splice
JSC	Photo	Pre	WL	1	T		
JSC	Photo	Pre	WL	2	T		
SOLAR IMAGES							
JSC	Photo	Post	WL	3	T		
JSC	Photo	Post	WL	4	T		
							1/2 in. wide splice, 1 in. wide gate
Sperry	X-Ray	Post	Al	166	T	21	Each step 5/16 in. wide, 5/8 in. normal from center to center, many steps touching
Sperry	X-Ray	Post	Ti	167	T	9	Same step size, normal spacing as Set 166
							1 in. wide gate
Sperry	UV	Post	2600		H	21	Each step 3/8 to 7/16 in. wide, 5/8 in. total spacing
Sperry		Post				1	
Sperry	Visible	Post	4000		H	21	Same as λ2600
Sperry	Visible	Post	5200		H	21	Same as λ2600
Sperry	Visible	Post	6400		H	21	Same as λ2600
							1 in. wide gate, 1/2 in splice, 1/2 in. splice
Aerospace	X-Ray	Post					Messed up, steps overlapping
↓ TAILS END							

TABLE 3-5. LOAD 4, IDENTIFICATION OF SENSITOMETRY SETS

ORIGIN OF SENSITOMETRY SET	TYPE OF SENSITOMETRY	PRE OR POST FLIGHT	SOURCE OR λ(A)	SET NO.	END OF SET WITH HIGH EXPOSURES	NUMBER OF STEPS (INTENDED OR ACTUAL)	REMARKS, STEP SIZE, OTHER FEATURES ON FILM
↑ HEADS END							
Sperry	UV	Pre	2600		H	21	Each step 3/8 to 7/16 in. wide, 5/8 in. from center to center
							~1 1/8 in. wide gate (?) (highly exposed)
Sperry	Visible	Pre	4000		H	21	Same as λ2600
Sperry	Visible	Pre	5200		H	21	Same as λ2600
Sperry	Visible	Pre	6400		H	21	Same as λ2600
							~2 in. wide, highly exposed section, 1 7/8 in. wide gate (?)
Sperry	X-Ray	Pre	Al	045-I	T	21	Each step 5/16 in. wide, 1 1/2 in. from center to center
Sperry	X-Ray	Pre	Al	045-II	T	21	Same as Set 045-I
							~7 in. highly exposed section
JSC	Photo	Pre	WL	1	T		
JSC	Photo	Pre	WL	2	T		
SOLAR IMAGES							
JSC	Photo	Post	WL	3	T		
JSC	Photo	Post	WL	4	T		
							1/2 in. wide splice, 6 1/2 in. highly exposed section, 1 in. wide gate
Sperry	X-Ray	Post	Al	256	T	22	Each step 5/16 in. wide, 1 1/2 in. from center to center
Sperry	X-Ray	Post	Cu	257	T	22	Same as Set 256
Sperry	X-Ray	Post	Ti	258	T	22	Same as Set 256
							1 1/4 in. wide gate
Sperry	UV	Post	2600		H	21	Each step 3/8 to 7/16 in. wide, 5/8 in. from center to center
Sperry	Visible	Post	4000		H	13	Same as λ2600
Sperry	Visible	Post	4000		H	21	Same as λ2600
Sperry	Visible	Post	5200		H	21	Same as λ2600
Sperry	Visible	Post	6400		H	21	Same as λ2600
							1 in. wide gate; "Marshall Sensi" 1/2 in. splice; "Aerospace Sensi"
Aerospace	X-Ray	Post	Cu	3	H	17	
Aerospace	X-Ray	Post	Al	2	H	17	Two lowest exposure steps overlap
Aerospace	X-Ray	Post	Al	1	H	16	
↓ TAILS END							

TABLE 3-6. LOAD 5, IDENTIFICATION OF SENSITOMETRY SETS

ORIGIN OF SENSITOMETRY SET	TYPE OF SENSITOMETRY	PRE OR POST FLIGHT	SOURCE OR λ(A)	SET NO.	END OF SET WITH HIGH EXPOSURES	NUMBER OF STEPS (INTENDED OR ACTUAL)	REMARKS, STEP SIZE, OTHER FEATURES ON FILM
↑ HEADS END							
JSC	Photo	Pre	WL	1	T		
JSC	Photo	Pre	WL	2	T		
SOLAR IMAGES							
JSC	Photo	Post	WL	3	T		
JSC	Photo	Post	WL	4	T		1/2 in wide splice, "Marshall Sensi", highly exposed mark (made by tape on flight film), 1 in. wide gate
Sperry	Visible	Post	6400		T	21	Each step 3/8 to 7/16 in. wide, 5/8 in. from center to center
Sperry	Visible	Post	5200		T	21	Same as λ6400
Sperry	Visible	Post	4000		T	21	Same as λ6400
Sperry	UV	Post	2600		T	21	Same as λ6400 1 in. wide gate
Sperry	X-Ray	Post	Ti	255	H	22	Each step 5/16 in. wide, 1 1/2 in. from center to center
Sperry	X-Ray	Post	Cu	254	H	22	Same as Set 255
Sperry	X-Ray	Post	Al	253	H	21	Same as Set 255 1 in. wide gate, 10 in. highly exposed section, 1/2 in. wide splice, "Aerospace Sensi"
Aerospace	X-Ray	Post	Al	1	T	21	
Aerospace	X-Ray	Post	Cu	2	T	18	
Aerospace	X-Ray	Post	Cu	3	T	13	2 1/2 in. long, medium exposed section, 1/2 in. wide splice, "227"
Sperry	X-Ray	Test	Al	227	H	12	1/2 in. wide splice, "226"
Sperry	X-Ray	Test	Al	226	H	12	
↓ TAILS END							

Test = Sensitometry set made on film which did not fly on Skylab.

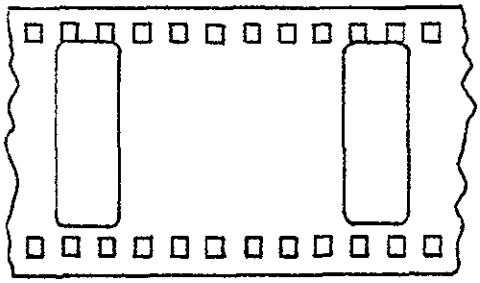

SPERRY X-RAY
LOADS 1,4,5 - ALL
LOADS 2,3 - PREFLIGHT ONLY

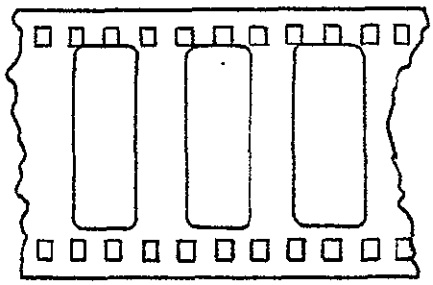

SPERRY X-RAY
LOADS 2,3 - POSTFLIGHT ONLY

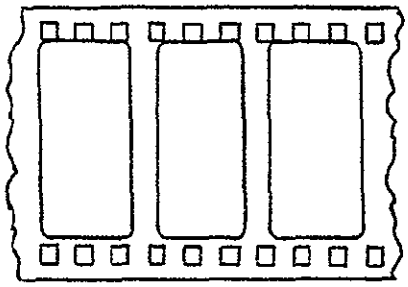

SPERRY VISIBLE, UV
ALL LOADS

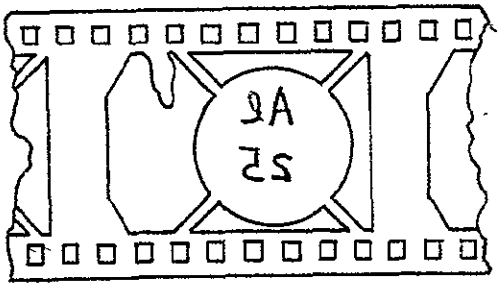

AEROSPACE X-RAY
LOAD 1

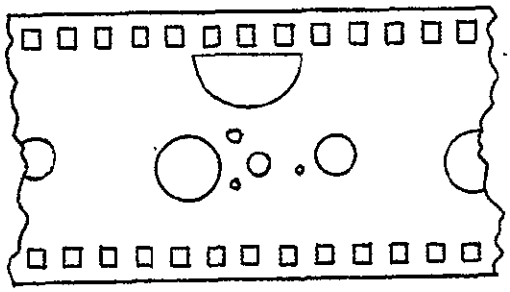

AEROSPACE X-RAY
LOADS 2,3,4,5

EMULSION IS DOWN ON FLIGHT FILM AND THIRD-GENERATION COPY, UP ON SECOND-GENERATION COPY. TAILS IS TO THE RIGHT IN ALL CASES EXCEPT AEROSPACE X-RAY LOAD 4 WHERE HEADS IS TO THE RIGHT.

FIGURE 3-3. APPEARANCE OF TYPICAL SENSITOMETRY SETS

3.4.2 Film Processing

Each of the loads of flight film was processed at JSC, typically approximately 2 weeks after splashdown for each mission. Before processing, segments of film were cut from each load, sent to MSFC and Aerospace for postflight sensitometry, and then returned to JSC and spliced back onto the rolls of film. Considerable effort was expended to guarantee uniform, high-quality development of the film. Information concerning the processing conditions for the film is given in Table 3-7.

After Load 1 was developed, a decision was made to develop the later loads of black-and-white film to a lower contrast. This accounts for the change in developing conditions for the SO-212 film shown in Table 3-7. Loads 2 and 3 were processed at the same time.

TABLE 3-7. S-056 FILM PROCESSING

LOAD	FILM TYPE	PROCESSOR	CHEMISTRY	TEMPERATURE (F)	DEVELOPING TIME (min:sec)	RATE (ft/min)
1	SO-212(B&W)	High-Speed	D-76	76	8:50	4
2	SO-212(B&W)	High-Speed	D-76	72	8:50	4
3	SO-212(B&W)	High-Speed	D-76	72	8:50	4
4	SO-212(B&W)	High-Speed	D-76	75	7:58	3.75
5	SO-242(Color)	Versamat 1811	EA-5	110(1st Dev.)	2:00	6

3.5 CALIBRATION RESULTS

This section contains an outline of the reduction and analysis of the sensitometric data described in Section 3.4 and then presents the resulting characteristic curves. Only the X-ray sensitometry was used in the calibration of the film.

3.5.1 Analysis of Sensitometric Data

Each exposure step in each sensitometry set was measured with a Macbeth TD-504 densitometer to obtain the doubley diffuse density. The

rolls of black-and-white film (Loads 1 through 4) were measured at Aerospace with a 2-mm-diameter aperture in the central portion of each step. Several measurements of each step were made to verify that the exposure and development had been uniform. The color film (Load 5) was measured at JSC with a 3-mm aperture; no color filter was used in the densitometer so that the density was measured with "white light".

The density readings were then plotted against the logarithm of the exposures (in photons per square centimeter) to obtain the conventional characteristic (H&D) curve plots. The photon flux was determined from the count rates measured by the proportional counters during the exposures in the sensitometer chambers. To convert count rate to photon flux, the counter aperture area and the distances between the X-ray source, counter, and film must be known.

All available X-ray data were plotted together for each load of film. In comparisons of the various sets of data, the aluminum (8.3 Å) data seemed to be the most consistent and reliable. There were, however, systematic differences between the Sperry and Aerospace data in that the Aerospace points lay to the right (toward higher exposures) of the Sperry points. Because the Aerospace proportional counters were operating continuously throughout their calibration exposures and because the Aerospace data for sources emitting different wavelengths were more consistent, it was decided to base the absolute calibration on the Aerospace sensitometry. The Sperry data covered a more extensive range of exposures and defined the shape of the curve better at high and low densities. Therefore, the procedure was to first draw a curve for each load based on the Sperry aluminum sensitometry and then to shift the curve to the right to agree with the Aerospace absolute values. The amount of the shift for a given load was calculated as the average displacement (in the logarithm of the exposure) between the Sperry curve and those Aerospace data points that were in or near the straight-line portion of the curve. Thus, the final characteristic curves are a composite of the Sperry and Aerospace sensitometry, with the shape of the curves being based on the Sperry data while the absolute values of the photon fluxes were derived from the Aerospace work.

3.5.2 Characteristic Curves and Related Data

The characteristic curves resulting from the analyses described in Section 3.5.1 are presented here in two forms. First, values of the logarithm of the exposure were read off the curves for many values of the density; these points are given in Tables 3-8 and 3-9. (Because Loads 2 and 3 were processed at the same time, the same curve applied to both loads.) In the toe and shoulder portions of the curves, the points are very closely spaced. In the straight-line portion of the curves, only the two end-points are given; thus, the positions and ranges of the straight-line regions are obvious from the large gap in data points. Linear interpolation can be used to calculate the logarithm of the exposure at any intermediate value of the density.

The second form of presentation of the curves consists of the plotted curves themselves as shown in Figures 3-4 through 3-7. The crosses are the points from Table 3-8 and 3-9 except that additional points are shown in the straight-line regions.

In the analysis of the X-ray photographs, it is often useful to have an analytical form for the characteristic curve for each roll of film. An attempt was made to fit several different kinds of expressions to the sensitometric data; the best formula was found to be a variation of that given by Green and McPeters (Ref. 3-9). The actual function used was

$$\log E = \log E_o + N(D-D_l) + K \log [1 - 10^{-(D-D_l)}] - M \log [1 - 10^{-(D_u-D)}],$$

where D is the doubly diffuse film density and E is the X-ray exposure in photons cm^{-2}. The data points to which the function was fitted are those plotted in Figures 3-4 through 3-7. The parameters, $\log E_o$, D_l, D_u, N, K, and M, resulting from the nonlinear least-squares fitting techniques are given in Table 3-10. The fitted curves are shown as the solid lines in Figures 3-4 through 3-7.

TABLE 3-8. CHARACTERISTIC CURVES, LOADS 1, 2, 3, AND 4

FLIGHT FILM DENSITY	log E (photons cm^{-2})		
	LOAD 1	LOADS 2 AND 3	LOAD 4
0.30	7.21		
0.32	7.51	6.645	
0.33		6.995	
0.34	7.71	7.165	
0.35		7.275	
0.36	7.84	7.355	
0.37		7.43	
0.38	7.93	7.49	
0.39		7.55	
0.40	8.01	7.605	
0.42		7.695	6.66
0.43			6.94
0.44		7.775	7.155
0.45	8.172		7.285
0.46		7.84	7.38
0.48		7.905	7.525
0.50	8.298	7.965	7.635
0.52		8.015	7.74
0.54			7.825
0.55	8.390	8.085	
0.56			7.885
0.58			7.945
0.60	8.468	8.185	7.995
0.62			8.045
0.64			8.09
0.65	8.538	8.268	
0.66			8.13
0.68			8.17
0.70	8.601	8.343	8.21
0.75	8.660	8.407	8.30
0.80	8.714	8.464	8.378
0.85	8.767	8.517	8.442
0.90	8.814	8.566	8.503
0.95		8.612	8.557
1.00	8.895	8.655	8.607
1.05		8.695	8.652
1.10	8.968	8.734	8.695
1.20	9.033	8.806	8.777
1.30	9.095		
1.40	9.153		
1.50	9.210		
2.40		9.636	9.664
2.50		9.710	9.745
2.60		9.788	9.828
2.70		9.872	9.918
2.80		9.963	10.017
2.90		10.062	10.123
3.00	9.993	10.173	10.234
3.05		10.233	10.292
3.10	10.046	10.296	10.352
3.15		10.364	10.411
3.20	10.107	10.435	10.472
3.25		10.516	10.533
3.30	10.174	10.609	10.60
3.35	10.210	10.715	10.67
3.40	10.248	10.847	10.745
3.45	10.291	11.007	10.795
3.47		11.082	
3.50	10.336		10.93
3.55	10.382		
3.56			11.10
3.60	10.433		
3.64			11.65
3.65	10.488		
3.70	10.551		
3.75	10.623		
3.80	10.702		
3.85	10.80		
3.90	10.94		

TABLE 3-9. CHARACTERISTIC CURVE, LOAD 5 (COLOR FILM)

FLIGHT FILM DENSITY*	log E (photons cm^{-2})	FLIGHT FILM DENSITY*	log E (photons cm^{-2})
2.47	7.668	0.65	9.818
2.46	7.833	0.60	9.866
2.45	7.938	0.55	9.919
2.44	8.013	0.50	9.973
2.42	8.122	0.45	10.033
2.40	8.199	0.40	10.097
2.38	8.264	0.35	10.171
2.36	8.320	0.30	10.252
2.34	8.373	0.28	10.285
2.32	8.415	0.26	10.321
2.30	8.457	0.24	10.359
2.25	8.545	0.22	10.404
2.20	8.616	0.20	10.447
2.15	8.680	0.18	10.502
2.10	8.738	0.16	10.558
2.05	8.791	0.14	10.623
2.00	8.839	0.12	10.702
1.90	8.926	0.10	10.792
1.80	9.005	0.09	10.853
1.70	9.078	0.08	10.913
1.00	9.537	0.07	10.992
0.90	9.608	0.06	11.105
0.80	9.686		
0.75	9.728		
0.79	9.772		

*Measured with no filter in densitometer.

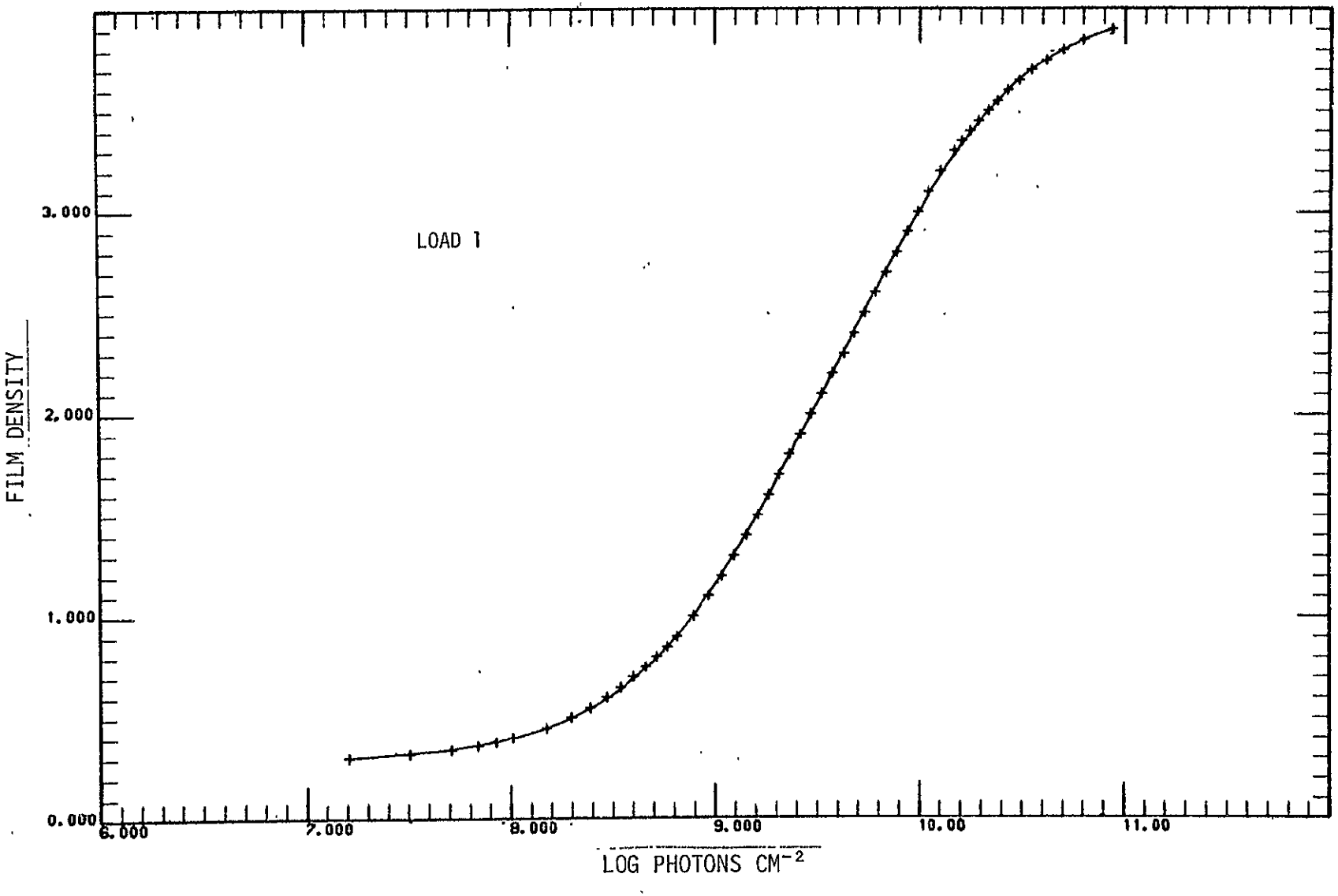

FIGURE 3-4. CHARACTERISTIC CURVE, LOAD 1

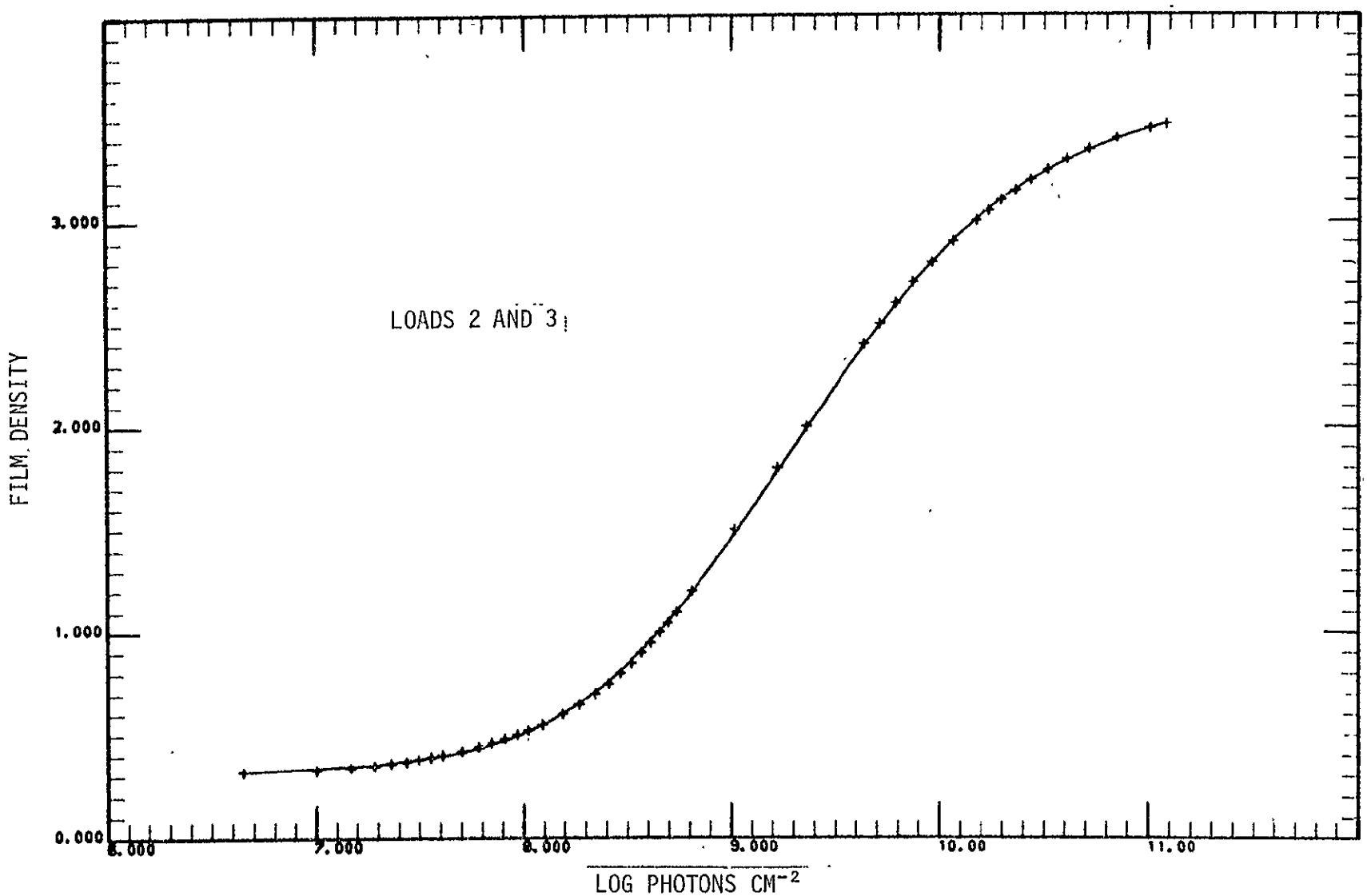

FIGURE 3-5. CHARACTERISTIC CURVE, LOADS 2 AND 3

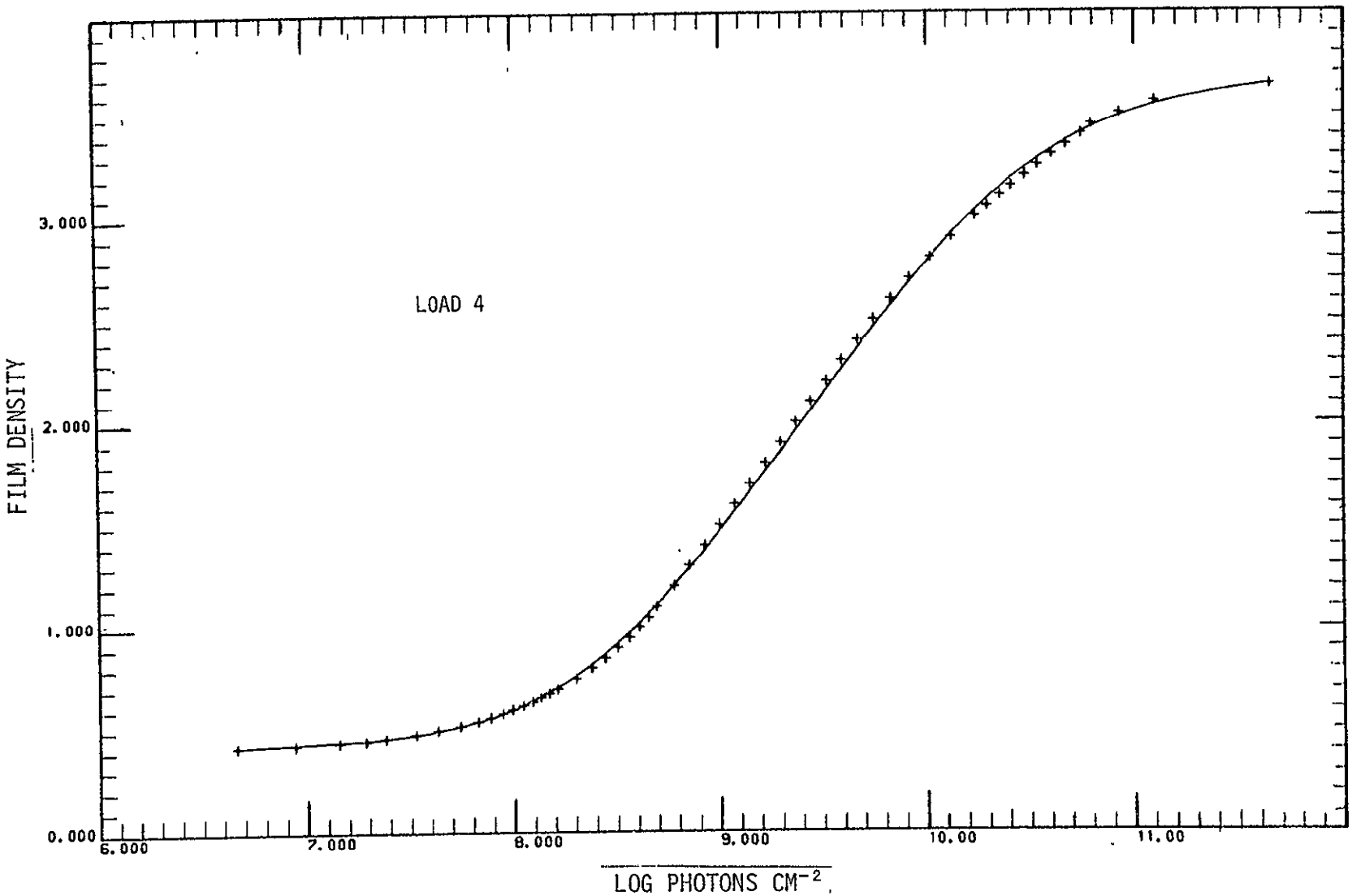

FIGURE 3-6. CHARACTERISTIC CURVE, LOAD 4

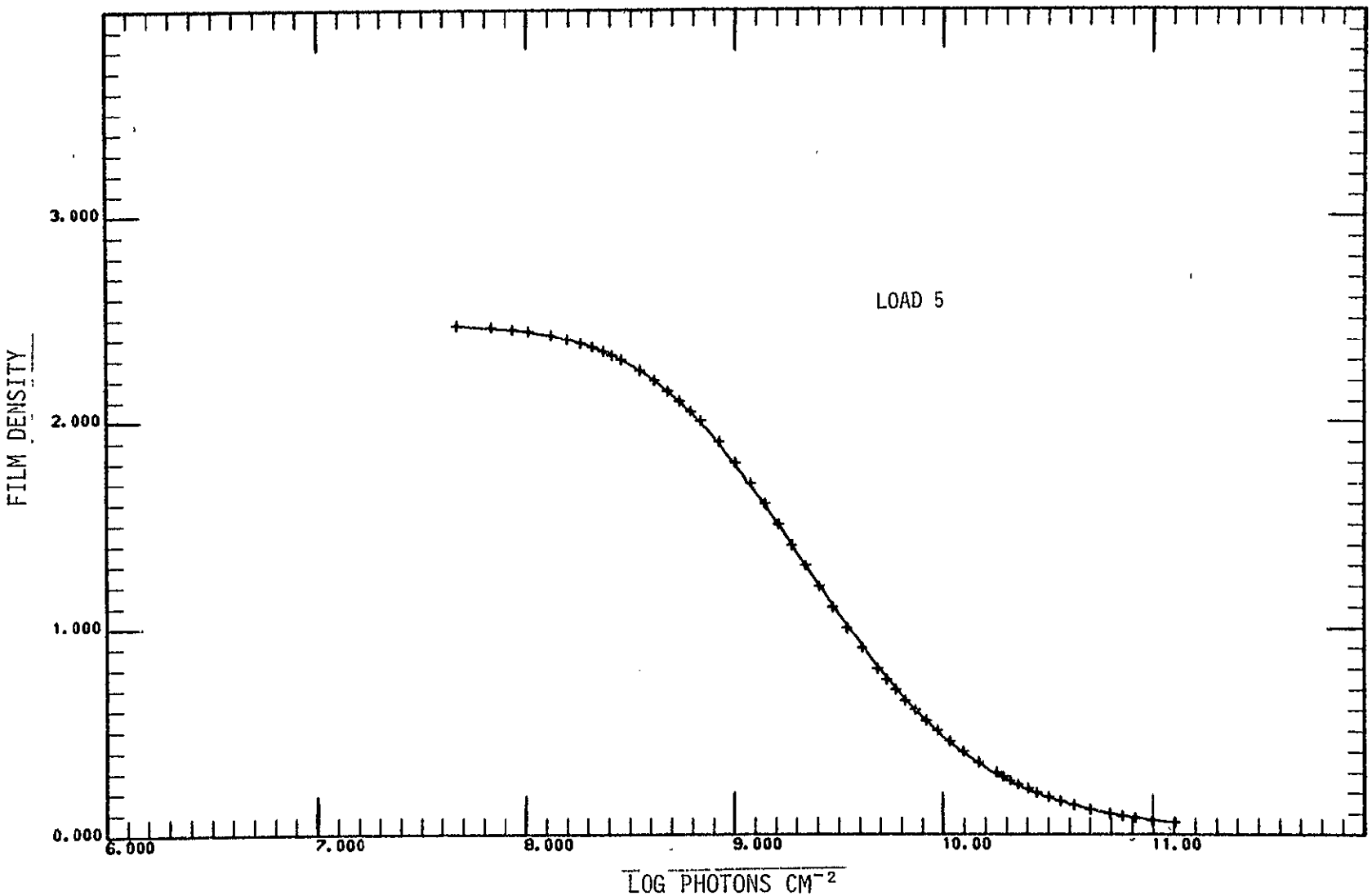

FIGURE 3-7. CHARACTERISTIC CURVE, LOAD 5 (COLOR FILM)

TABLE 3-10. PARAMETERS FOR CHARACTERISTIC CURVE FITS

	LOAD 1	LOADS 2 AND 3	LOAD 4	LOAD 5 (COLOR)
$\log E_o$	8.6410	8.3349	8.3063	10.0626
D_u	4.0122	3.6934	3.6996	2.4856
D_l	0.2756	0.3080	0.4113	0.0094
N	0.4846	0.6047	0.6873	-0.5611
K	1.1383	1.0632	.9787	-1.0959
M	0.8515	2.1066	1.2374	-0.6946

Certain commonly used parameters relating to the characteristic curves are listed in Table 3-11. These parameters include the background or base plus fog density, the contrast (gamma), and the speed of each load. For the black-and-white loads, the fog is highest on Load 4, which was exposed to the Skylab environment for the longest time. The speed is given according to three different definitions as explained in the table.

To simplify the transfer of the calibration results from the flight films to any copies that may be used, a "standard" sensitometry set has been selected for each load and provided the appropriate exposure values in Table 3-12. Each standard set is a Sperry set, and its location may be found with the aid of Tables 3-2 through 3-6. The densities of the steps in each standard set may be measured in any system or by any device as long as the same system or device is used for the measurement of the solar images. Use of Table 3-12, thus, does not depend on any particular copy, in contrast to Tables 3-8 and 3-9 or Figures 3-4 through 3-7, which apply only to the flight films themselves.

TABLE 3-11. CHARACTERISTIC CURVE PARAMETERS

	LOAD 1	LOADS 2 AND 3	LOAD 4	LOAD 5 (COLOR)
Gamma	1.92	1.45	1.35	-1.53
Base + Fog Density	0.29	0.31	0.41	2.48
Speed(0.1)	1.07(-8)	2.24(-8)	2.04(-8)	5.45(-9)
Speed(1.0)	8.15(-10)	1.31(-9)	1.17(-9)	5.99(-10)
Speed(B+F)	2.64(-9)	6.45(-9)	6.41(-9)	2.71(-9)

The speeds are defined as the reciprocal of the exposure in photons per square centimeter at the points:
(0.1) - on the curve at a density of 0.1 above* base plus fog
(1.0) - on the curve at a density of 1.0 above* base plus fog
(B+F) - at the intersection of the straight-line portion (extrapolated downward) with the base plus fog-level.

* Below base plus fog for Load 5.

All of the preceding data are given in units of photons per square centimeter for the X-ray exposure of the film, independent of the wavelength, as was discussed in Section 3.3.1. Because the final absolute calibration was tied primarily to the aluminum (8.34 Å) exposures, the photon flux (photons/cm^2) can be converted to energy flux (ergs/cm^2) by simply multiplying each exposure value in photons by 2.382×10^{-9} (the number of ergs per photon at 8.34 Å).

3.6 USE OF COPY FILMS

To avoid damage to the original flight film, it has not been used for scientific analyses except in a limited number of cases.

TABLE 3-12. EXPOSURE VERSUS STEP NUMBER FOR STANDARD SENSITOMETRY SETS

STEP NO. FROM HIGH EXPOSURE END	EXPOSURE (photon cm^{-2})				
	LOAD 1 SET 106	LOAD 2 SET 047-I	LOAD 3 SET 048-I	LOAD 4 SET 256	LOAD 5 SET 253
	↑ HEADS	↑ TAILS	↑ TAILS	↑ TAILS	↑ HEADS
1	5.97(10)	3.05(10)	4.06(10)	3.31(11)	1.30(11)
2	2.99(10)	1.81(10)	2.10(10)	1.66(11)	6.49(10)
3	1.49(10)	8.99(9)	9.62(9)	8.28(10)	3.24(10)
4	7.46(9)	4.12(9)	4.79(9)	4.14(10)	1.62(10)
5	3.76(9)	2.15(9)	2.40(9)	2.07(10)	8.11(9)
6	1.81(9)	1.05(9)	1.15(9)	1.04(10)	4.06(9)
7	1.38(9)	7.38(8)	8.26(8)	4.97(9)	2.87(9)
8	9.29(8)	5.22(8)	5.89(8)	3.64(9)	1.97(9)
9	6.53(8)	3.76(8)	4.09(8)	2.50(9)	1.39(9)
10	4.65(8)	2.62(8)	2.91(8)	1.72(9)	9.93(8)
11	3.27(8)	1.85(8)	2.06(8)	1.22(9)	6.98(8)
12	2.32(8)	1.31(8)	1.46(8)	8.55(8)	4.97(8)
13	1.67(8)	9.40(7)	1.05(8)	6.08(8)	3.56(8)
14	1.16(8)	6.53(7)	7.31(7)	4.40(8)	2.48(8)
15	7.98(7)	4.49(7)	5.04(7)	3.10(8)	1.71(8)
16	5.81(7)	3.27(7)	3.66(7)	2.15(8)	1.24(8)
17	4.36(7)	2.92(7)	2.74(7)	1.57(8)	9.31(7)
18	2.90(7)	2.60(7)	1.83(7)	1.17(8)	6.21(7)
19	2.18(7)	1.22(7)	1.37(7)	7.82(7)	4.66(7)
20	1.45(7)	8.17(6)	9.14(6)	5.87(7)	3.10(7)
21	7.26(6)	4.08(6)	9.14(6)	3.91(7)	1.55(7)
22			4.57(6)	1.95(7)	
	↓ TAILS	↓ HEADS	↓ HEADS	↓ HEADS	↓ TAILS

Instead, copies have been produced for scientific analyses of the solar images and for submission to the National Space Science Data Center (NSSDC). The analyses include densitometry for quantitative work and the preparation of photographic prints.

The first attempts at copying the black-and-white film at JSC met with difficulty, primarily because of the large density range on the original (with densities up to almost 4.0). The copies, and the prints and transparencies made from them, showed only the features with intermediate exposure; the high and low intensity features were lost. Therefore, a series of tests of candidate copy materials and methods of development was undertaken at Aerospace. The desired properties were low contrast and large exposure range. The film finally chosen for the second-generation copies of the black-and-white film (Loads 1 through 4) was Kodak Type 5235, a panchromatic separation film; these copies are positives and were made at Aerospace. Unfortunately, the film still could not be made to yield the required range of exposure in a single copy. Two different versions were made, a high-exposure copy for bright X-ray features and low-exposure copy (with exposure approximately 4 stops less than that received by the high-exposure copy) for faint features. These two different exposure copies are therefore known as bright-feature and faint-feature versions. The two copies also differ in the contrast (γ) to which they were developed. The bright-feature copy was developed to $\gamma \approx 0.7$ so as not to saturate the high intensity areas, and the faint-feature copy was developed to $\gamma \approx 1.0$ to enhance the contrast of the faint features.

Many third-generation negative copies of Loads 1 through 4 have also been made at Aerospace and JSC. These copies have been made on several films, including Kodak Types 5366, 5234, and 5235. They are not used for quantitative work but are very convenient for examination or any use where extremely careful handling is not required.

Black-and-white and color copies have been made of the color film (Load 5), primarily at JSC. Because the flight or first-generation film was a color-reversal film, the second-generation black-and-white copies

are negative copies. Again, bright-feature and faint-feature versions were made. The film was Kodak Type 2402, a Plus-X aerographic film with a panchromatic emulsion having extended red sensitivity. Third-generation positive copies were then made on Kodak Type 5366, a duplicating positive film. The third-generation copies were normally exposed copies of each of the bright-feature and faint-feature versions of the second-generation films.

In addition to the ordinary black-and-white copies of Load 5, color-separation copies were made by Technicolor. The second-generation color-separation copies are black-and-white negatives made on Kodak Type 5234, a duplicating panchromatic negative film. Three separate copies were made with cyan, yellow, and magenta filters. The primary reason for making the color-separation copies was to preserve the color information on the color film. Initially, it appeared that the densities on the original were changing; however, this problem has been alleviated with the storage of the original color film in a dry, refrigerated environment.

Color copies have also been made of Load 5. Second- and third-generation copies were made on Kodak Type 5389, an Ektachrome-R color-reversal print film. Copies with a number of different exposures were made to show the entire range of exposures on the original.

The copies of each of the five loads that have been sent to NSSDC are black-and-white positives in the bright-feature and faint-feature versions. For Loads 1 through 4, they are second-generation copies; for Load 5, they are third-generation copies.

REFERENCES - SECTION 3

3-1. J. H. Underwood, J. E. Milligan, A. C. deLoach, and R. B. Hoover, "S-056 X-Ray Telescope Experiment on the Skylab Apollo Telescope Mount", Applied Optics, Vol. 16, pp. 858-869, 1977

3-2. R. Haggerty, R. Simon, L. Golub, J. K. Silk, A. F. Timothy, A. S. Krieger, and G. S. Vaiana, "Soft X-Ray Imaging on Photographic Film", AAS Photo-Bulletin No. 10, pp. 8-14, 1975

3-3. Kodak Aerial Films and Photographic Plates, Eastman Kodak Company Publication No. M-61, Rochester, New York, 1975

3-4. R. L. Light and H. W. Lollar, "Summary Report of Photographic Film Testing for ATM Experiment S-056", Technical Report No. SP-580-0501, Sperry Rand Corporation, 1971

3-5. J. H. Underwood, "NASA Final Report on the Scientific and Technical Support for ATM Experiment S-056", Aerospace Corporation Report No. ATR-76(7405)-6, 1976

3-6. R. Simon, R. Haggerty, L. Golub, A. S. Krieger, J. K. Silk, A. F. Timothy, and G. S. Vaiana, "Response of Photographic Film to Soft X-Ray Radiation", American Science and Engineering Report No. ASE-3775

3-7. "Kodak Aerial Color Film (Estar Thin Base) SO-242, Kodak Aerial Color Film (Estar Ultra-Thin Base) SO-255", Eastman Kodak Company, Publication No. M-74, revision, 1973

3-8. L. C. Clune, W. F. Waite, and J. A. Gordon, "Measurement of Soft X-Ray Photon Energies with Color Photographic Film", AAS Photo-Bulletin No. 10, pp. 3-7, 1975

3-9. A. E. S. Green and R. D. McPeters, "New Analytic Expressions of Photographic Characteristic Curves", Applied Optics, Vol. 14, pp. 271-272, 1975

4. MORPHOLOGY AND PHYSICAL PARAMETERS OF A SOLAR FLARE

(An altered version of a paper published in The Astrophysical Journal, Vol. 216, pp. L79-L82, September 1, 1977)

Authors

J. B. Smith, Jr.
NOAA/SEL; Presently Located at Marshall Space Flight Center

R. M. Wilson
NASA - Marshall Space Flight Center

W. Henze, Jr.
Teledyne Brown Engineering
Huntsville, Alabama

4.1 INTRODUCTION

The flare of June 15, 1973 was one of the best observed flares of the Skylab mission and has been selected for concentrated study by the Skylab Workshop on Solar Flares. This section briefly describes the Hα, magnetic, and X-ray morphology and evolution of the flare and its source active region and present temperatures and electron densities for the flaring plasma based on data obtained by the ATM S-056 X-ray experiment on Skylab.

Preflare and early flare observations show photospheric and chromospheric changes not previously discussed. The early flare development of an arch filament and the observation of new following polarity spots in the vicinity of the site of flare onset are evidence of emerging magnetic flux. This section also describes the preflare and early flare filament activation disappearance observed with the event. These types of activity have frequently been associated with flare occurrence (Ref. 4-1).

The X-ray observations used to determine physical parameters include both photographic images and proportional counter data. The spatially resolved images yield effective line-of-sight temperatures $\bar{T}$ and electron densities N_e, whereas the full-Sun proportional counter data have high time resolution and provide time profiles of the flux and the effective parameters over the flare volume.

4.2 X-RAY INSTRUMENTATION

The NASA-Marshall Space Flight Center/The Aerospace Corporation X-ray telescope experiment (S-056) aboard Skylab consisted of two separate instrument systems: 1) the X-Ray Telescope (X-RT) and 2) the X-Ray Event Analyzer (X-REA). The X-RT, a glancing-incidence, imaging X-ray telescope system, obtained filterheliograms through five metallic, broad-band X-ray filters of different bandpass in the 6-to-18-Å and 27-to-40-Å range with varying exposure times (generally between 1.25 sec and 5 min) and with high spatial resolution ($\sim$2 in.). The X-REA included two sealed,

gas-filled proportional counters employing pulse-height analyzers for spectral resolution and viewed the full Sun with a temporal resolution of 2.5 sec. Spectral ranges were 2.5 to 7.25 Å and 6.1 to 20 Å. The instruments have been described in more detail in Refs. 4-2 and 4-3.

4.3 OBSERVATIONS

The source of the two-ribbon 1B/M3 flare was a simple bipolar region but with some complexity introduced by the elongated, almost isolated intrusion of leader polarity into the trailing portion of the region (Figure 4-1a). In the days preceding the flare, the spot group had declined, with only a single leader spot observed early on June 15. The Hα plage had also declined in intensity, and flare production had been sporadic, consisting of occasional subflares with minor X-ray events for the previous 5 days and no reported flares (other than faint subflares) for 72 hours prior to the discussed event.

The chromospheric (Hα) and coronal (X-ray) structure of the active region about 1 hour prior to flare onset is shown in Figures 4-1c and 4-1d. At that time, the plage was slightly enhanced and the dark, embedded, northeast-southwest oriented filament was intermittently active. The visible coronal structure consisted primarily of an arcade of loops joining the zones of opposite polarity. The northernmost bright arched feature was oriented approximately southeast-northwest, extending from the position of the horseshoe-shaped (open south) trailing-polarity Hα plage element to the northern portion of the leading plage. Its projected dimensions were about 15 by 60 in. Force-free (curl $B = \alpha B$) coronal magnetic field lines have been calculated for various values of α, and we find that a spatially varying α is required to best fit the X-ray coronal observations. The calculated potential field ($\alpha = 0$) is shown in Figure 4-1b.

The flare of June 15, despite being of moderate size in Hα and of only moderate X-ray intensity, was of particular interest as the first relatively large event of Skylab and as one of the best observed

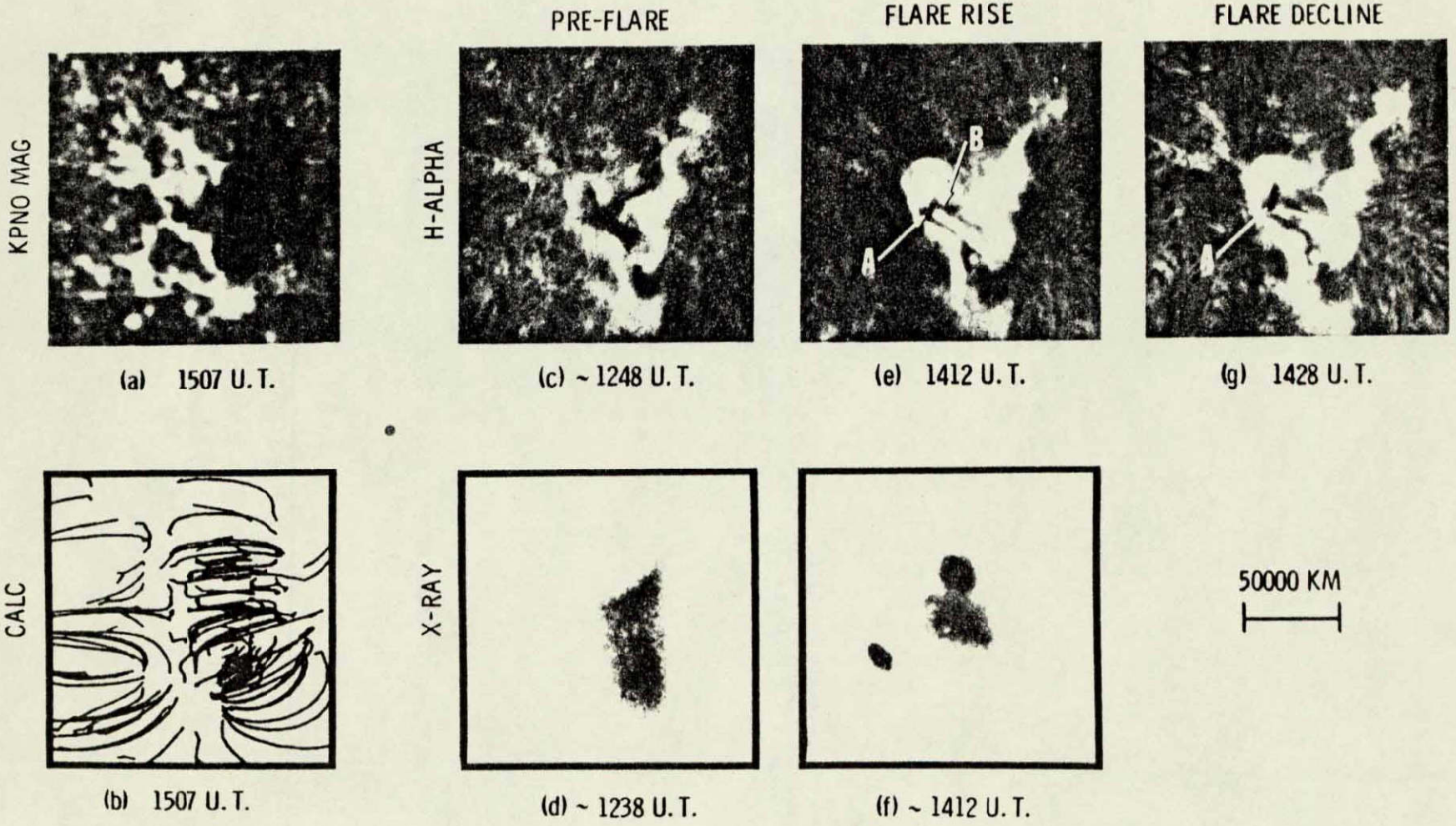

FIGURE 4-1. FLARE OF 1973 JUNE 15. (a) the KPNO magnetogram and (b) the calculated potential field; (c) Hα preflare, (e) late in the flare rise, and (g) during the decline; (d) X-ray photographs pre-flare (8-18 Å, 29.25 s) and (f) during the flare rise (6-12 Å, 4.4 s). The bright spots near the flare in (f) are data block lights.

4.4 PHYSICAL PARAMETERS

To infer physical parameters for the flaring plasma, the filter-ratio method (Ref. 4-6) has been applied to the X-ray photographs. A similar technique was employed in the analysis of the proportional counter data. For the X-RT, the basic observed quantities are the integrals of the specific intensity over the transmission functions of the various filters. The X-REA measures the flux integrated over the proportional counter response functions for the various channels. It is assumed that the X-ray emission comes from coronal regions that are optically thin and isothermal, either along the line of sight (for the X-RT photographs) or over the entire coronal flare volume (for the X-REA data). Theoretical X-ray emission spectra given in References 4-7 and 4-8 are used, as applied to the S-056 instrumental response stated in Reference 4-9.

Under our assumptions, the ratio of the integrals of the intensity or flux for different filters or channels is a function of temperature only. The observed intensity and the theoretical emission at the temperature inferred from the ratio are then used to determine either the linear or volume emission measure which, for an assumed geometry, yields the number density. Potential inaccuracies in temperatures determined from soft X-ray data are discussed in References 4-9 and 4-10.

Results of physical parameter determination from analysis of X-RT photographic data are shown in Table 4-1. Following a preflare calculated temperature of 3.2×10^6 K, the effective temperature based on the ratio of filters with passbands of 6 to 12 Å and 8 to 14 Å reached a peak of 25×10^6 K (with possible errors estimated at $\pm 5 \times 10^6$ K), using deconvolved data (as compared to 20×10^6 K prior to deconvolution) at 1415 UT, the approximate time of peak flux in all filters. However, the X-REA observations, with better time resolution (Figures 4-2 and 4-3), show a peak spectral hardness (and a peak temperature) 3 to 4 min earlier and a peak in the 2.5-to-4.5-Å flux at 1414 UT. Temperatures calculated by ratioing 1-min averages of channels covering the wavelength ranges 2.5 to 3.75 Å and 3.75 to 4.5 Å show an initial rise to approximately

TABLE 4-1. JUNE 15, 1973 FLARE PHYSICAL PARAMETERS AT POINT OF PEAK X-RAY EMISSION

	PREFLARE (1244 UT)	FLARE (~1415 UT)	POSTFLARE (1740 UT)
T (K)	3.2×10^6	25×10^6	3.5×10^6
EM (cm^{-5}) ($=\int N_e^2 dl$)	2.5×10^{28}	1.5×10^{30}	1.3×10^{28}
N_e (cm^{-3})	4.7×10^9	4.5×10^{10}	3.4×10^9
	(dl ~11,000 km)	(dl ~7400 km)	(dl ~11,000 km)

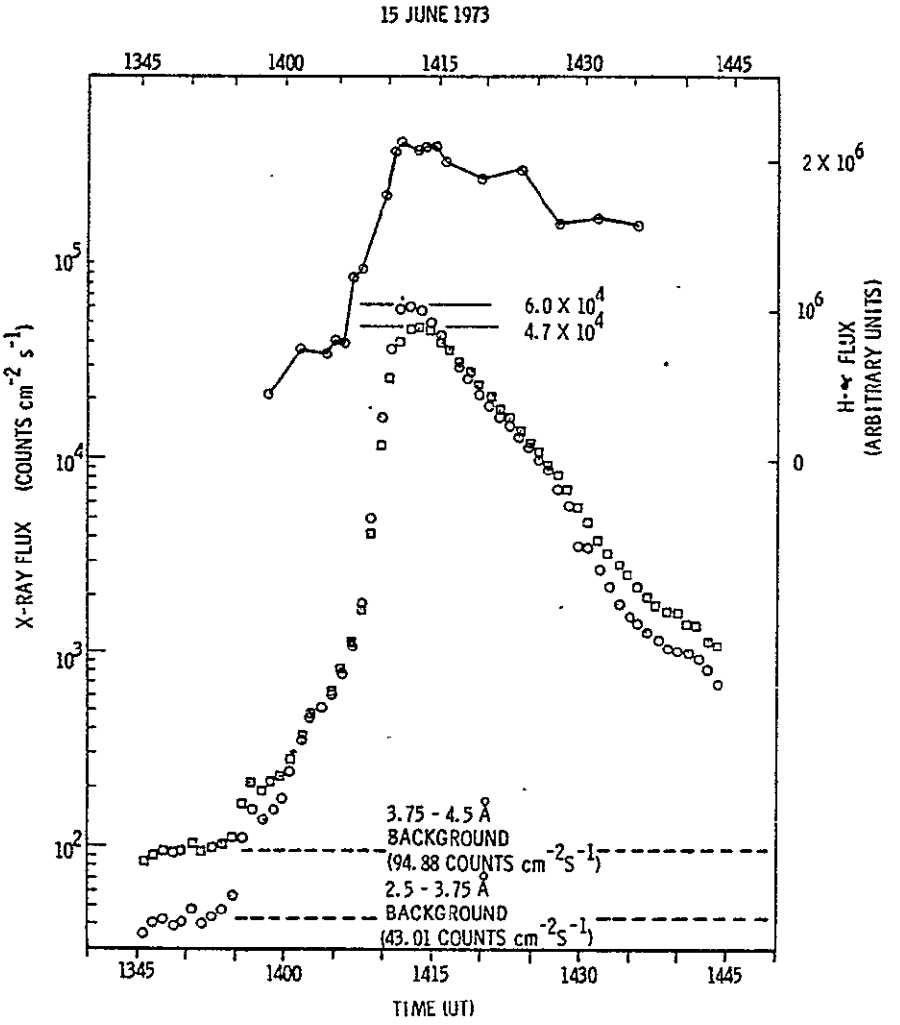

FIGURE 4-2. Hα AND X-REA FLUX PROFILES

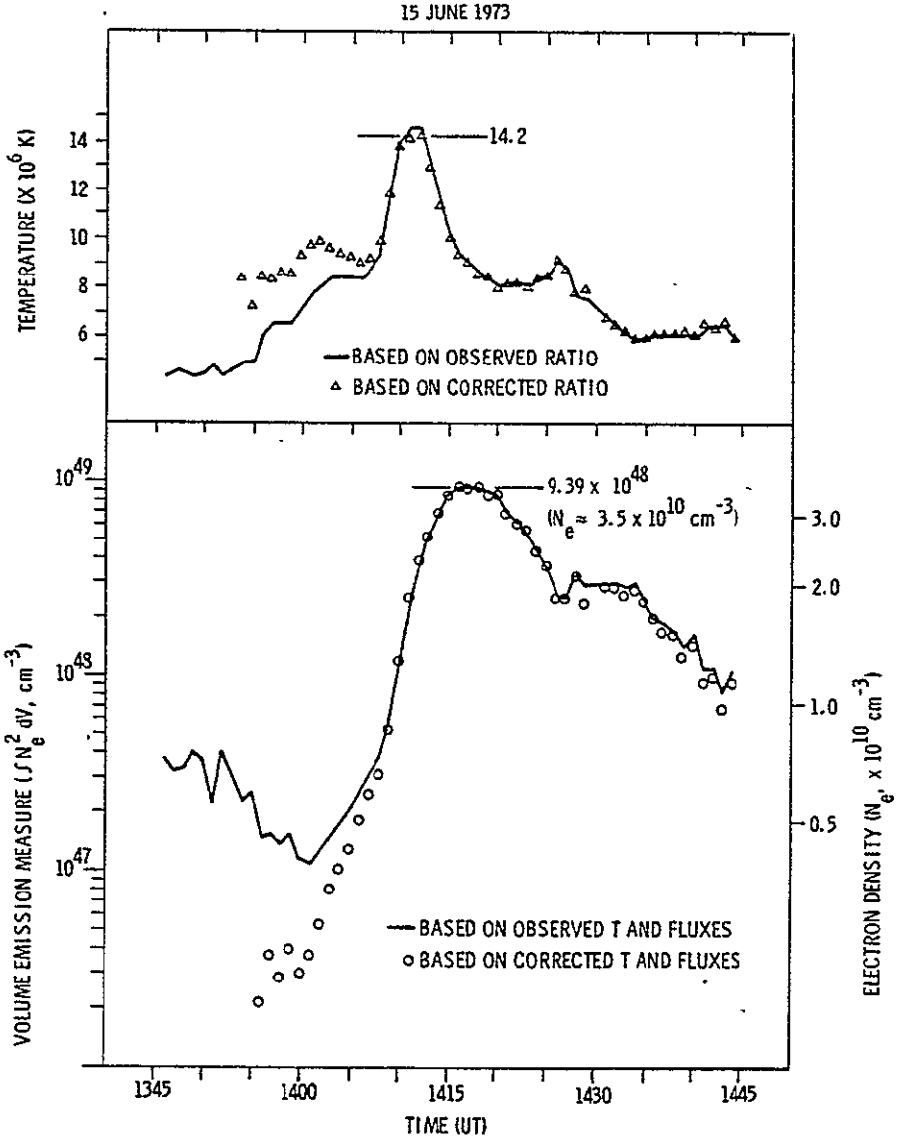

FIGURE 4-3. TEMPERATURE AND DENSITY PROFILES DERIVED FROM X-REA DATA. THE CORRECTED CURVES HAVE BACKGROUND REMOVED.

9×10^6 K at approximately 1402 UT, indicating preflash-phase heating. (Possible internal errors in X-REA determined temperatures are estimated at ±10%.) The temperature then remains nearly constant until approximately 1407 UT, the apparent beginning of the flash phase, when it rises rapidly to a peak of 14.2×10^6 K at 1411 to 1412 UT. (The 2.5-sec data show a brief maximum of 16.5×10^6 K approximately 1411.5 UT.) Other investigators have calculated comparable temperatures for this event. For example, a maximum temperature of 16×10^6 K from SOLRAD 10 soft X-ray observations was reported in Reference 4-11. More recently, Reference 4-12 reported calculated maximum temperatures of approximately 13×10^6 K by ratioing Fe XXIII and Fe XXIV emission and 16.2×10^6 K using SOLRAD-9 data.

Assuming cylindrical symmetry of a flaring flux tube, the tube diameter was estimated to be 10 in., or approximately 7,400 km. This length is used as the line-of-sight thickness for the determination of density from the X-RT images. It is also combined with the observed area of the X-ray flare to obtain the volume of 7.5×10^{27} cm^3 used for deriving the density from the X-REA data. As shown in Table 4-1, N_e inferred from the images increases to 4.5×10^{10} cm^{-3} while the X-REA data yield 3.5×10^{10} cm^{-3} (Figure 4-3), with the maximum occurring about 2 min after the peak soft X-ray flux. The number density peak following flare maximum is typical of X-ray flares (Ref. 4-13).

4.5 DISCUSSION

The observation of embedded filament activity and the strong implication of emerging flux are further evidence for the occurrence of these types of activity preceding and accompanying flares. In particular, it appears that active region filaments must be taken into account in any viable flare model.

This section has presented determinations of the temperature of a solar flare based 1) on Skylab spatially resolved X-ray observations and 2) on full-disk proportional-counter data. The maximum temperature

calculated from the imaged X-RT data is of the order of 25×10^6 K. This line-of-sight temperature is larger than the peak temperature of 14.2×10^6 K (for the entire flare volume) obtained from the X-REA data; if real, a possible explanation is that the X-REA observations include more plasma at lower temperatures. Evidence has been found for preflash-phase heating to $\sim 9 \times 10^6$ K in this event; such heating, though much discussed, has not been frequently observed in the past. A maximum electron density of $\sim 3.5 \times 10^{10}$ cm^{-3} has been calculated using X-REA data at 4.5×10^{10} cm^{-3} from X-RT data, values which are comparable to those reported by others for this and other flares.

REFERENCES - SECTION 4

4-1. J. Heyvaerts, E. R. Priest, and D. M. Rust, Ap. J., 1977 (in press)

4-2. J. H. Underwood, J. E. Milligan, A. C. deLoach, and R. B. Hoover, Appl. Opt., 16, p. 858, 1977

4-3. R. M. Wilson, NASA-MSFC Technical Memorandum X-73332, 1976

4-4. J. B. Smith, Jr., Solar Activity Observations and Predictions, ed., P. S. McIntosh and M. Dryer, Cambridge: MIT Press, p. 429

4-5. D. M. Rust, Solar Phys., 47, p. 21, 1976

4-6. G. S. Vaiana, A. S. Krieger, and A. F. Timothy, Solar Phys., 32, p. 81, 1973

4-7. A. B. C. Walker, Jr., Space Sci. Rev., 13, p. 672, 1972

4-8. W. H. Tucker and M. Koren, Ap. J., 168, p 283, 1971

4-9. J. H. Underwood and D. L. McKenzie, Solar Phys. (in press)

4-10. I. J. D. Craig and J. C. Brown, Astr. Ap., 49, p. 239, 1976

4-11. K. G. Widing and C. C. Cheng, Ap. J. (Letters), 194, p. LIII, 1974

4-12. K. G. Widing and K. P. Dere, submitted to Solar Phys., 1977

4-13. D. W. Datlowe, H. S. Hudson, and L. E. Peterson, Solar Phys., 35, p. 193, 1974

5. ANALYSIS OF X-RAY OBSERVATIONS OF THE 15 JUNE 1973 FLARE IN ACTIVE REGION NOAA 131: PLASMA DIAGNOSTICS

(Extracted from an Article Submitted to Solar Physics)

Authors

K. R. Krall
School of Science and Engineering
University of Alabama in Huntsville

E. J. Reichmann
R. M. Wilson
NASA - Marshall Space Flight Center

W. Henze, Jr.
Teledyne Brown Engineering
Huntsville, Alabama

J. B. Smith, Jr.
NOAA/SEL; Presently Located at Marshall Space Flight Center

The filter-ratio method of analysis of broadband X-ray filter images to obtain physical parameters of solar features has been described in Reference 5-1. A similar technique has been used for proportional counter or ionization chamber (SOLRAD) observations (Ref. 5-2). In this section, these methods has been adapted to our own observations.

The exposure on the film, Φ_n (in photons cm^{-2}, where n denotes the filter), at any point in an image formed by an X-ray telescope is related to the specific intensity, I_λ, by:

$$\Phi_n = \frac{At}{f^2} \int \eta_n (\lambda) \frac{I_\lambda(\lambda)}{h\nu} d\lambda \qquad (5\text{-}1)$$

where

- A - telescope collecting area
- t - exposure time
- f - telescope focal length
- $\eta_n(\lambda)$ - combined filter-telescope transmission for photons of wavelength λ
- $h\nu$ - energy per photon.

For an optically thin plasma of coronal composition and temperature, assumed to be isothermal along the line of sight, Equation 5-1 becomes

$$\Phi_n = \frac{At}{f^2} \int \eta_n(\lambda) \frac{\varepsilon_\lambda(\lambda)}{N_e^2 h\nu} d\lambda \int N_e^2 \, d\ell, \qquad (5\text{-}2)$$

where

- $\varepsilon_\lambda(\lambda)$ - emission coefficient
- N_e - electron density
- ℓ - distance along the line of sight
- $\int N_e^2 \, d\ell$ - linear emission measure

Theoretical solar X-ray emission spectra (Refs. 5-3 and 5-4) applied to the S-056 instrumental response (Ref. 5-5) are used. When Equation 5-2

is evaluated for two different filters, the theoretical ratio of the right-hand sides depends only on the temperature. The temperature can be determined from the observed ratio of the quantities Φ_n. Once the temperature is known, the linear emission measure is found by using Equation 5-2 for either filter. The electron density is obtained from the emission measure with an assumption about the geometrical extent along the line of sight. Although the filter-ratio method just described has been the standard technique for the interpretation of broadband filter images, other approaches based on models of the temperature variation of the differential emission measure are now being investigated (Ref. 5-5).

A similar formulation can be developed for proportional counter observations with a field of view containing the entire Sun. With the assumption that the plasma is isothermal over the flare volume, the equivalent to Equation 5-2 is:

$$\Psi_n = \frac{At}{(AU)^2} \int \eta_n(\lambda) \frac{\varepsilon_\lambda(\lambda)}{N_e^2 \, h\nu} \, d\lambda \int N_e^2 \, dV \qquad (5\text{-}3)$$

where

Ψ_n - number of counts in channel n

AU - astronomical unit

V - volume

$\int N_e^2 \, dV$ - volume emission measure.

The aperture area, A, the integration time, t, and $\eta_n(\lambda)$, the number of counts in channel n per photon at wavelength λ, are analogous to the corresponding quantities in Equation 5-2. The observed X-REA fluxes to be presented later are the values of Ψ_n/At, which are equal to the integrals over wavelength of the photon flux at the Earth multiplied by the response functions for the various channels. The temperature, volume emission measure, and electron density are obtained in a manner similar to that described above for the telescope images.

REFERENCES - SECTION 5

5-1. G. S. Vaiana, A. S. Krieger, and A. F. Timothy, Solar Phys., 32, p. 81, 1973

5-2. D. M. Horan, Solar Phys., 21, p. 188, 1971

5-3. A. B. C. Walker, Space Sci. Rev. 13, p. 672, 1972

5-4. W. H. Tucker and M. Koren, Astrophys. J. 168, p. 283, 1971

5-5. J. H. Underwood and D. L. McKenzie, submitted to Solar Phys., 1977

6. TIME-VARYING OSCILLATIONS IN THE SOLAR SOFT X-RAY FLUX AS OBSERVED FROM SKYLAB

(An altered version of an article submitted to Astronomy and Astrophysics)

Authors

D. L. Teuber
R. M. Wilson
NASA - Marshall Space Flight Center

W. Henze, Jr.
Teledyne Brown Engineering
Huntsville, Alabama

6.1 INTRODUCTION

The initial discovery of quasi-periodic oscillations in the solar atmosphere (i.e., the now familiar 300-sec oscillation) was made by Leighton and his colleagues in 1960 (Refs. 6-1 through 6-3). Several other investigators quickly confirmed the notion of "oscillatory motion" in the photospheric and chromospheric regions and provided a more detailed account of the oscillations (Refs. 6-4 through 6-7). Recent reviews by Michalitsanos (Ref. 6-8) and Stein and Leibacher (Ref. 6-9) discuss the theoretical interpretation of the observed oscillations.

Evidence for solar oscillations (262-sec period) in the transition region and lower corona, based on the EUV lines of He II (304 Å), Mg VIII (315 Å), and Mg IX (368 Å) as observed by OSO-7, was first reported by Chapman et al. (Ref. 6-10). In addition, Jakimiec and Jakimiec (Ref. 6-11) found quasi-periodic oscillations of the 1-to-8-Å solar X-radiation (based on SOLRAD 9 data), with periods ranging from 200 to 900 sec, and Chipman et al. (Ref. 6-12) reported evidence of 300-sec and longer oscillations, based on a study of the Si II (1816 Å) line observed by OSO-8. In contrast, Vernazza et al. (Ref. 6-13), while seeing intensity changes up to 50% in times as short as 1 min in the EUV lines of H I (1216 Å), C II (1336 Å), C III (977 Å), O IV (554 Å), O VI (1032 Å), and Mg X (625 Å) as observed by the Harvard experiment aboard Skylab, failed to find periodic oscillations in these lines, with the possible exception of a 300-sec oscillation in the lines of H I and C II. Recent radio measurements (Refs. 6-14 through 6-16), however, suggest that quasi-periodic oscillations with periods from 1 min up to possibly several hours do exist in the chromospheric and coronal regions.

To search for periodic variations in coronal X-ray emission, observations have been examined that were obtained by the Skylab/ATM S-056 X-ray experiment. In this section, evidence is presented for the existence of time-varying oscillations of the X-ray flux during a flare.

6.2 OBSERVATIONAL RESULTS

Full-disk proportional counter data from the X-REA, which was part of the ATM/S-056 experiment were used. The data pertain to the flare of June 15, 1973 (Refs. 6-17 and 6-18) and to two "quiet" periods, one following the flare and the other on August 15, 1973 when the Sun was extremely quiet with no large active regions on the disk. The X-REA consisted of two sealed, gas-filled counters operating over the 2.5-to-7.25-Å and 6.1-to-20-Å wavelength ranges. The 2.5-to-7.25-Å counts were separated into six energy channels by the use of pulse-height analysis. Similarly, the 6.1-to-20-Å counts were separated into four energy channels. In this analysis, the 2.5-to-3.75-Å channels were used. A discussion of the overall ATM/S-056 experiment is given in Reference 6-19; for a detailed description of the X-REA and how to reduce its data, see References 6-20 and 6-21.

The observations consist of count rates measured every 2.5 sec by the aforementioned proportional counters. The maximum number of samples was about 1400, based on the 1-hr daylight portion of the Skylab orbit. A cosine-bell Hanning filter was applied to the first and last 10% of each set of data. To increase the spectral resolution, zeros were added to extend the number of samples to 2048; the resulting frequency resolution was 0.195 mHz, corresponding to a period of 85 min for the first spectral element. The power spectrum was then computed for each event using the Fast Fourier Transform algorithm.

The observed count rate in the 2.5-to-3.75-Å channel for the interval, including the June 15, 1973 1B/M3 flare is shown in Figure 6-1 along with the power spectrum computed from the data. Only the first 240 spectral elements have been plotted, out to a frequency of 0.047 Hz. The low-frequency components below spectral element number 10 (where zero frequency is at spectral number 1) represent the large-scale rise and decay of the flare emission. There is a prominent peak at spectral number 21 corresponding to a period of 256 sec. Another peak occurs at three times the first frequency, corresponding to a period of 85 sec. The power contained in the peak around 256 sec is of the order of 2 to 3%.

To determine whether the oscillations are associated with the flare or whether they might be instrumental in origin, the power spectra for two other intervals were computed. The observed count rate and its associated power spectrum are shown in Figure 6-2 for the interval later on June 15, 1973, when a number of active regions were present on the disk but no flares were reported. The same proportional counter channel was used as that which provided the flare data in Figure 6-1. A shorter total interval was used as shown in Figure 6-2 to exclude the rise and to avoid the data gap. Although there is again a peak at a period of 256 sec in the power spectrum in Figure 6-2, it is not as pronounced as the peak in Figure 6-1. The data obtained on August 15, 1973, an extremely quiet day with no large active regions on the disk, are shown in Figure 6-3. Because the count rate was so low in the 2.5-to-3.75-Å range, it was decided to use the 8-to-12-Å channel in the analysis. The 2.5-to-3.75-Å data were used in the analysis of the June 15 event because the oscillations were more clearly visible; the 8-to-12-Å data also showed the oscillations but to a lesser extent.) It is clear that there is no significant maximum rising above the noise in the power spectrum.

6.3 DISCUSSION AND CONCLUSIONS

The peak at the period of 256 sec in Figure 6-1 agrees well with the periods of 278 sec in SOLRAD X-ray emission found by Reference 6-11 and 262 sec in EUV lines found by Reference 6-10. Both sets of X-ray data are full-disk observations obtained during flares; however, the EUV data were obtained in quiet regions near the center of the disk. The existence of oscillations in the X-ray flux during flares may be explained by waves generated during the flare. Such waves would periodically increase the electron density (N_e) and the temperature and thus increase the emission, which is proportional to N_e^2 and is a strong function of temperature for the highest-energy proportional-counter channel used. Although oscillations are also present in other channels, they are strongest in the 2.5-to-3.75-Å channel shown in Figure 6-1.

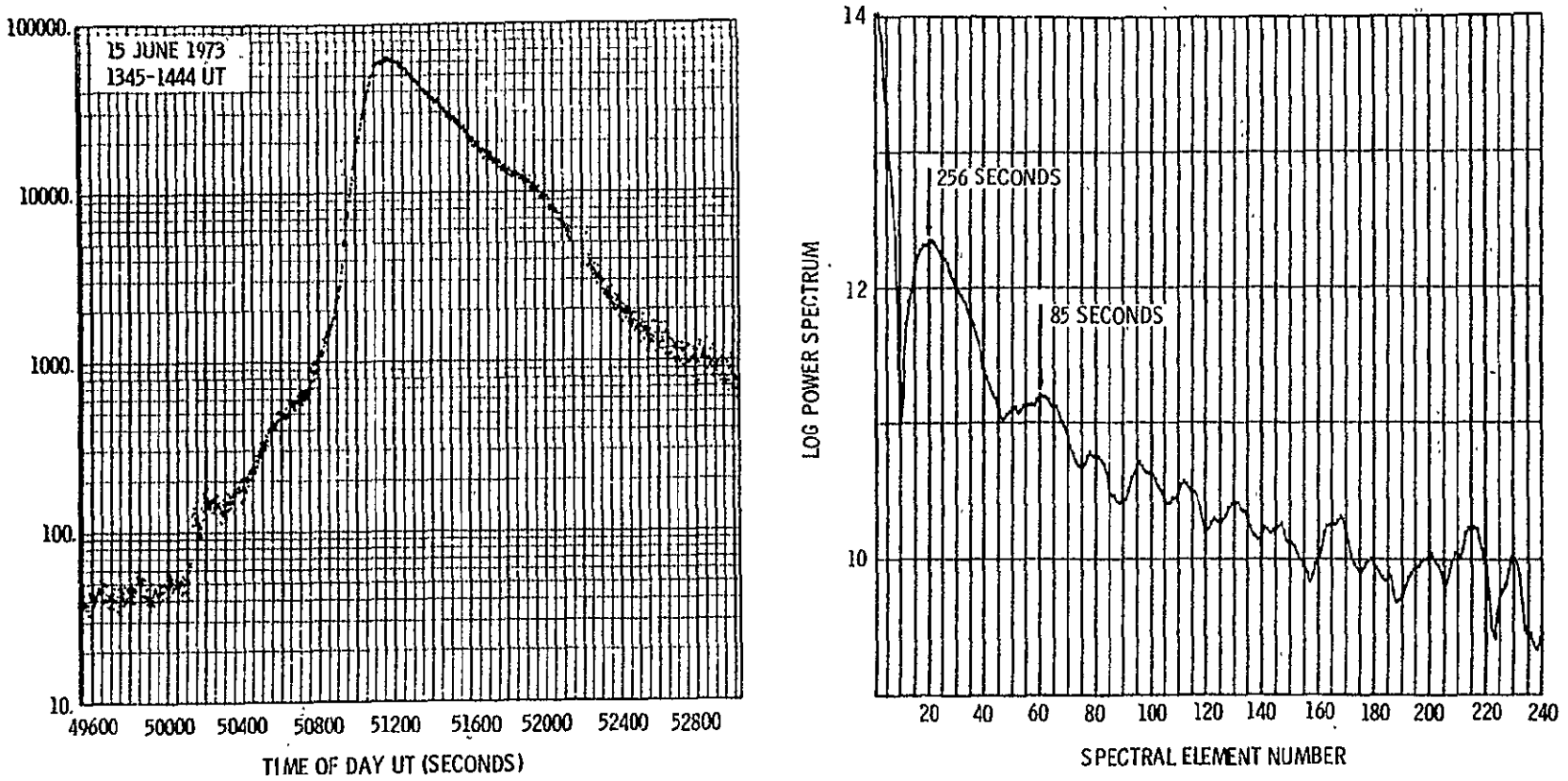

FIGURE 6-1. TIME VARIATION AND POWER SPECTRUM OF SOLAR X-RAY FLUX, 2.5-TO-3.75-Å CHANNEL, JUNE 15, 1973, 1345-1444 UT

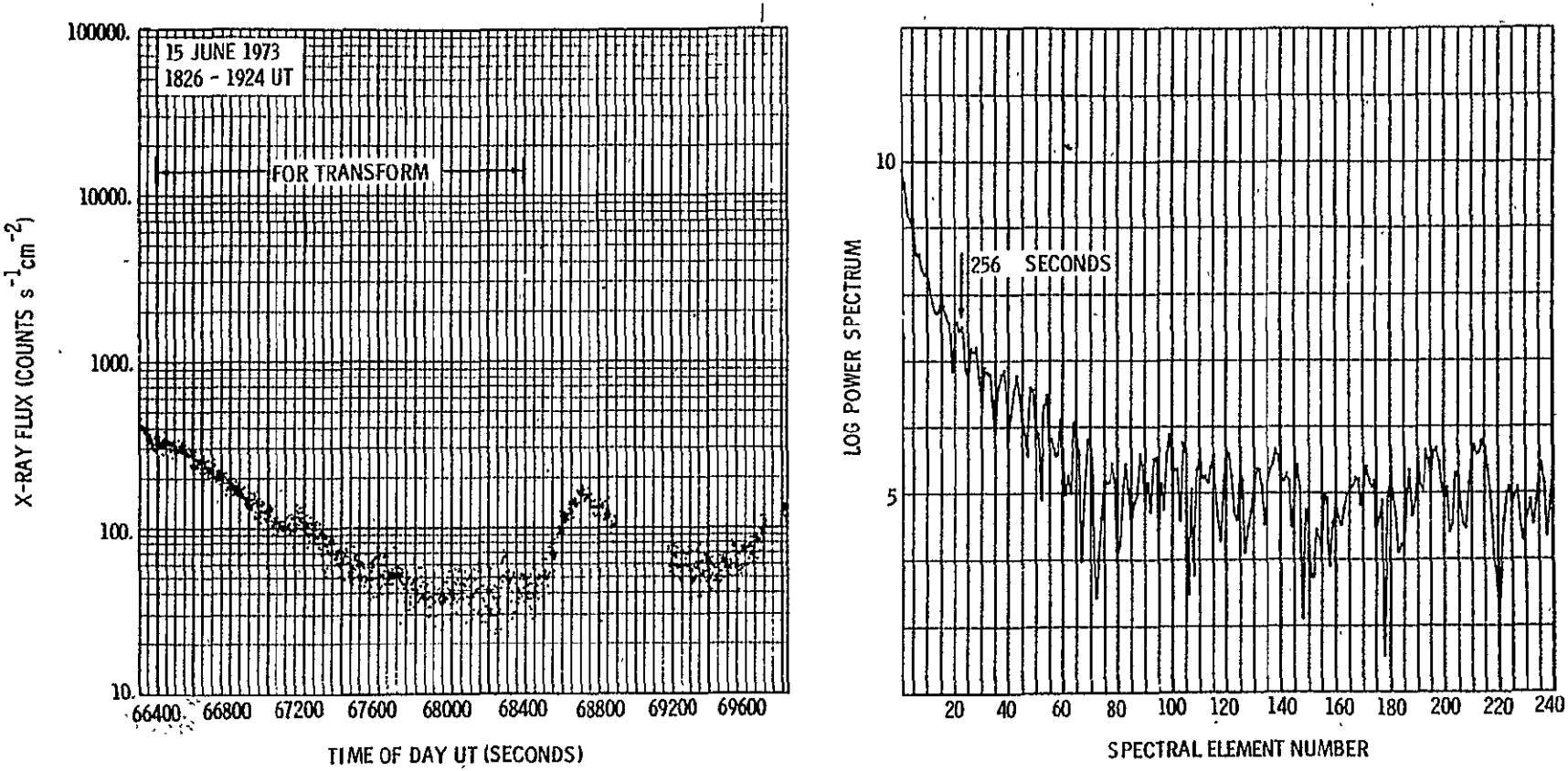

FIGURE 6-2. TIME VARIATION AND POWER SPECTRUM OF SOLAR X-RAY FLUX, 2.5-TO-3.75-Å CHANNEL, JUNE 15, 1973, 1826-1924 UT

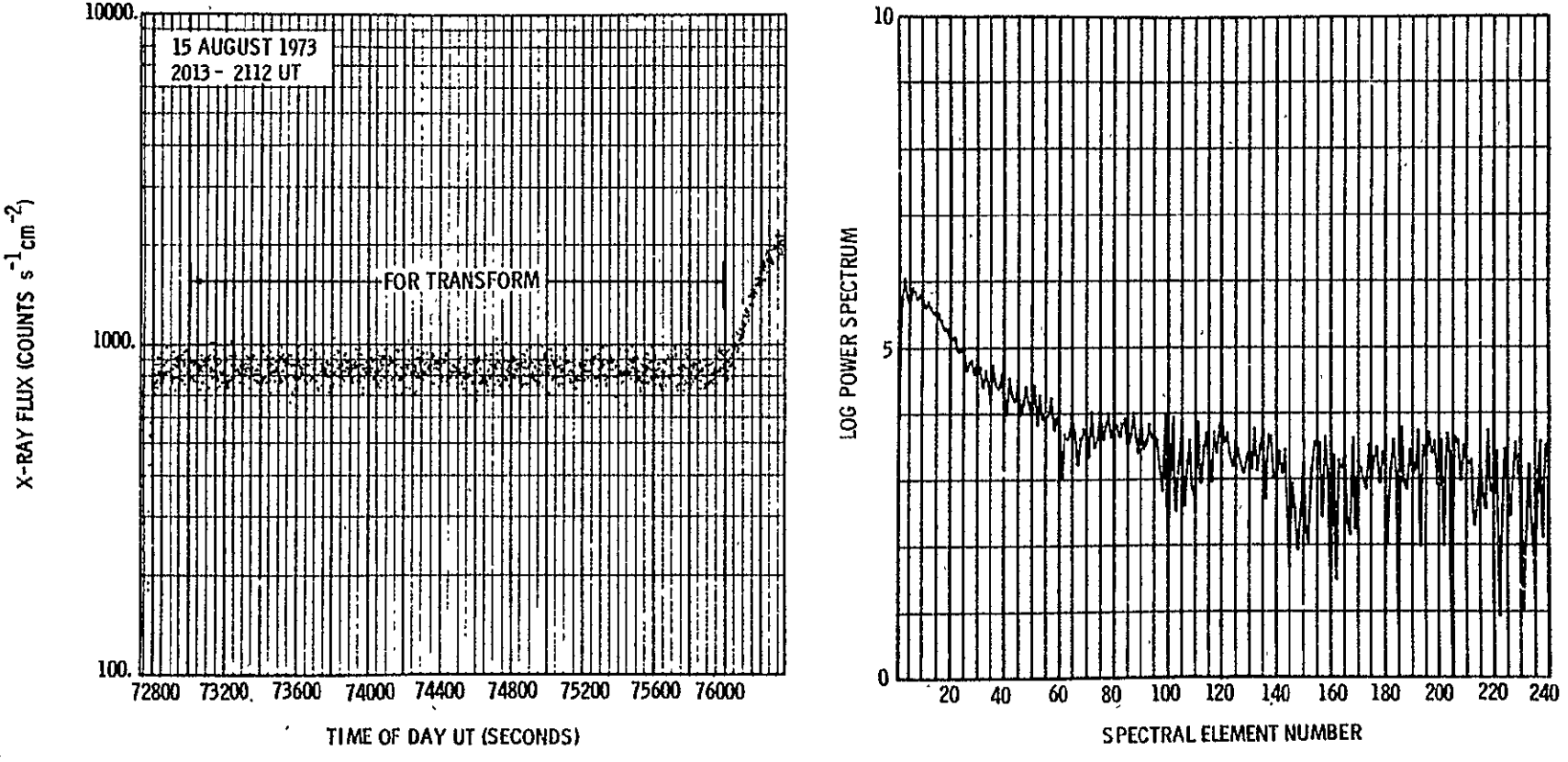

FIGURE 6-3. TIME VARIATION AND POWER SPECTRUM OF SOLAR X-RAY FLUX, 8-TO-12-Å CHANNEL, AUGUST 15, 1973, 2013-2112 UT

In conclusion, oscillations were detected in the soft X-ray flux from a solar flare. Because no oscillations have been observed in the flux during quiet periods, it was concluded that the oscillation is not instrumental and is related to the flare. Additional flares will be examined to determine whether oscillations are characteristic of all flares or of only certain classes of flares. It is also planned to investigate other types of solar transient events such as eruptive prominences and preflare intervals.

REFERENCES - SECTION 6

6-1. R. B. Leighton, Nuovo Cimento Suppl. 22, p. 321, 1961

6-2. R. B. Leighton, R. W. Noyes, and G. W. Simon, Astrophys. J. 135, p. 474, 1962

6-3. R. W. Noyes and R. B. Leighton, Astrophys. J. 138, p. 631, 1963

6-4. J. W. Evans and R. Michard, Astrophys. J. 136, p. 493, 1962

6-5. E. Jensen and F. Q. Orrall, Astrophys. J. 138, p. 252, 1963

6-6. E. N. Frazier, Astrophys. J. 152, p. 557, 1968

6-7. F. L. Deubner, Astron. & Astrophys. 44, p. 371, 1975

6-8. A. G. Michalitsanos, Earth and Extraterrestrial Sci. 2, p. 125, 1973

6-9. R. F. Stein and J. Leibacher, Ann. Rev. Astron. Astrophys. 12, p. 407, 1974

6-10. R. D. Chapman, S. D. Jordan, W. M. Neupert, and R. J. Thomas, Astrophys. J. (Letters) 174, p. L97, 1972

6-11. J. Jakimiec and M. Jakimiec, Astron. & Astrophys. 34, p. 415, 1974

6-12. E. G. Chipman, E. C. Bruner, R. A. Shine, B. W. Lites, and G. J. Rottman, Bull. Am. Astr. Soc. 7, p. 522, 1975

6-13. J. E. Vernazza, P. V. Foukal, M. C. E. Huber, R. W. Noyes, E. M. Reeves, E. J. Schmahl, J. G. Timothy, and G. L. Withbroe, Astrophys. J. (Letters) 199, p. L123, 1975

6-14. M. S. Durasova, M. M. Kobrin, and O. I. Judin, Nature Phys. Sci. 229, p. 83, 1971

6-15. L. W. Avery, Solar Phys. 49, p. 141, 1976

6-16. M. M. Kobrin, V. V. Pakhomov, and N. A. Prokof'eva, Solar Phys. 50, p. 113, 1976

6-17. J. B. Smith, Jr., R. M. Wilson, and W. Henze, Jr., Astrophys. J. (Letters) 216, p. L79, 1977

6-18. K. R. Krall, E. J. Reichmann, R. M. Wilson, W. Henze, Jr., and J. B. Smith, Jr., Solar Phys. (submitted), 1977

6-19. J. H. Underwood, J. E. Milligan, A. C. deLoach, and R. B. Hoover, Appl. Opt. 16, p. 858, 1977

6-20. R. M. Wilson, NASA/Marshall Space Flight Center Technical Memorandum X-73332, 1976

6-21. R. M. Wilson, NASA/Marshall Space Flight Center Technical Memorandum X-73367, 1977

7. DECONVOLUTION OF S-056 X-RAY IMAGES OF THE SEPTEMBER 5, 1973 FLARE

The true distribution of intensity from any source is changed when passing through an observing system so that the resulting image distribution will be different. In many cases, the change is small so that the observed distribution can be considered to be nearly the same as the true distribution. However, the question of whether observed images do or do not need correction for instrumental effects must be investigated for each case. This section describes the results of such an investigation for the photographic images obtained by the S-056 X-ray telescope.

The observed intensity is usually expressed as the convolution of the true object distribution and the instrumental point-spread function. The recovery of the true distribution is called deconvolution and is usually performed with Fourier transforms. The mathematical details were given in an earlier contract report (Ref. 7-1).

The on-axis S-056 point-spread function used in deconvolution was also given in an earlier report (Ref. 7-2). It has a sharp core with full width at half maximum of approximately 2 arc-sec and broad wings caused by zonal aberrations and scattering from the surfaces of the mirrors.

Photographic images of the September 5, 1973 flare were scanned, converted to intensity units through the characteristic curve of the film, filtered with a lowpass filter, and then deconvolved; all steps were performed using the Image Data Processing System (IDAPS) at MSFC (Ref. 7-3). During the flare, the S-056 telescope operated in the active mode so that only Filters 1, 3, and 5 were used. All available images during a period of about 7 min were scanned. The results for the peak intensity in the flare images are shown in Figure 7-1. The figure shows the variation with time of the peak intensity through each of the three filters and compares the nondeconvolved and deconvolved cases.

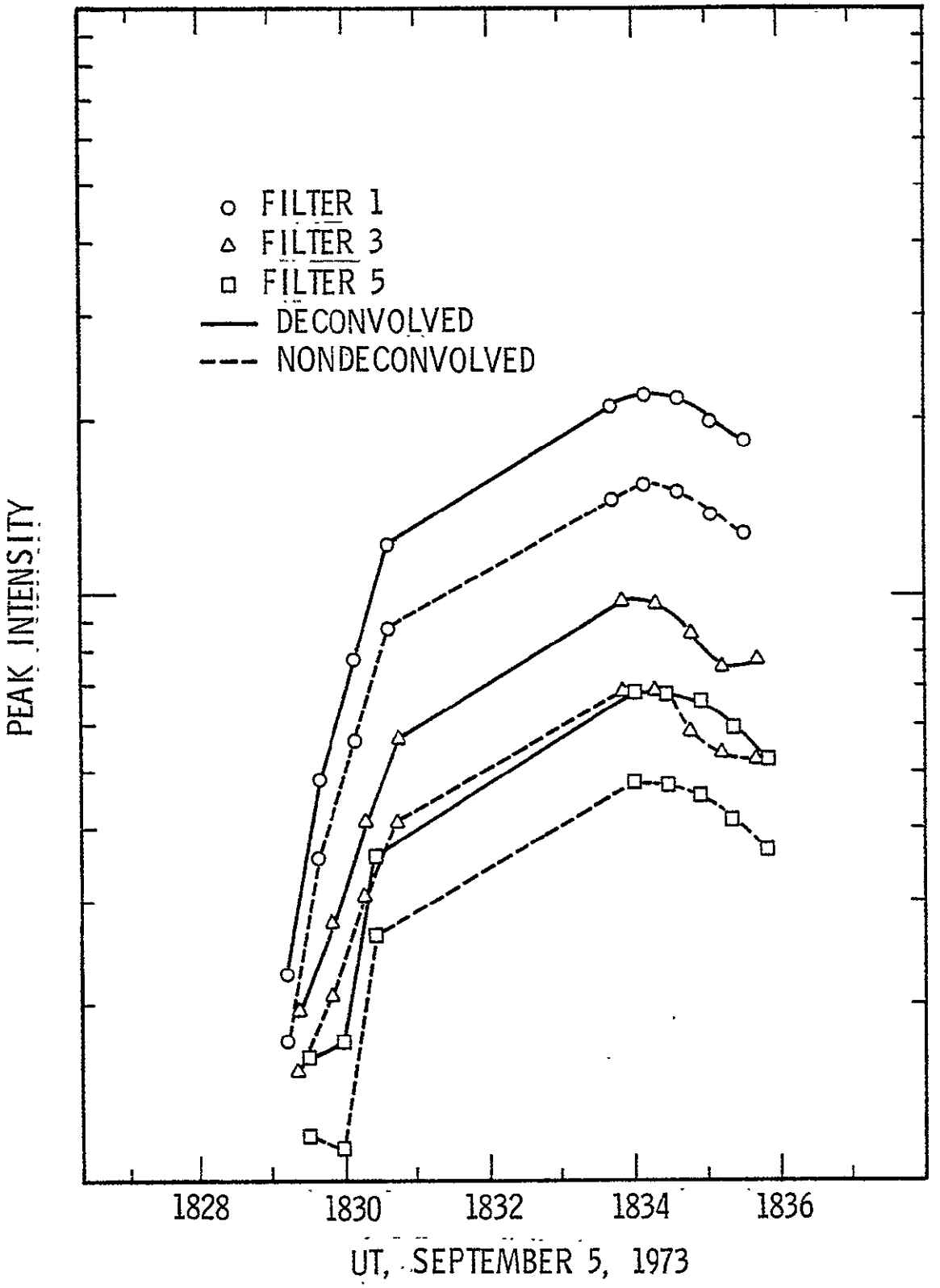

FIGURE 7-1. VARIATION OF PEAK INTENSITY DURING SEPTEMBER 5, 1973 FLARE

A general conclusion that is evident from the figure is that the peak intensity is increased by about 40% in all filters when the image is deconvolved. Thus, the ratio of the peak intensities at any time for any two of the three filters would not change, and any temperature information inferred from the filter ratios would not change. Therefore, it is concluded that for the brightest portions of the S-056 images, no deconvolution is required when filter ratios are used.

Using the data shown, it is difficult or impossible to infer any significant variation in the temperature during the flare; if anything, the temperature, under the isothermal approximation, appeared to be slightly lower at the peak of the flare. The brightness using Filter 1 appeared to be too high. If the ratio of Filter 5 to Filter 3 is used, temperatures of 7×10^6 to 10×10^6 K and emission measures of 10^{29} to 10^{30} cm^{-5} are obtained. If the thickness is 10^4 km, the density is 1×10^{10} to 3×10^{10} cm^{-3}.

REFERENCES - SECTION 7

7-1. W. Henze, Jr., "Solar Radiometry at Millimeter Wavelengths", Teledyne Brown Engineering Interim Report EE-SSL-1812, 1974

7-2. W. Henze, Jr., "Research in Solar Physics", Teledyne Brown Engineering Final Report SD76-MSFC-2040, 1976

7-3. R. M. Wilson, D. L. Teuber, J. R. Watkins, D. T. Thomas, and C. M. Cooper, "Image Data-Processing System for Solar Astronomy", Applied Optics 16, pp. 947-949, 1972